JGP Journal of General Physiology

ARTICLE

Molecular rearrangements in S6 during slow inactivation in *Shaker*-IR potassium channels

Tibor G. Szanto[1], Ferenc Papp[1], Florina Zakany[1], Zoltan Varga[1], Carol Deutsch[2], and Gyorgy Panyi[1]

Voltage-gated K^+ channels have distinct gates that regulate ion flux: the activation gate (A-gate) formed by the bundle crossing of the S6 transmembrane helices and the slow inactivation gate in the selectivity filter. These two gates are bidirectionally coupled. If coupling involves the rearrangement of the S6 transmembrane segment, then we predict state-dependent changes in the accessibility of S6 residues from the water-filled cavity of the channel with gating. To test this, we engineered cysteines, one at a time, at S6 positions A471, L472, and P473 in a T449A *Shaker*-IR background and determined the accessibility of these cysteines to cysteine-modifying reagents MTSET and MTSEA applied to the cytosolic surface of inside-out patches. We found that neither reagent modified either of the cysteines in the closed or the open state of the channels. On the contrary, A471C and P473C, but not L472C, were modified by MTSEA, but not by MTSET, if applied to inactivated channels with open A-gate (OI state). Our results, combined with earlier studies reporting reduced accessibility of residues I470C and V474C in the inactivated state, strongly suggest that the coupling between the A-gate and the slow inactivation gate is mediated by rearrangements in the S6 segment. The S6 rearrangements are consistent with a rigid rod-like rotation of S6 around its longitudinal axis upon inactivation. S6 rotation and changes in its environment are concomitant events in slow inactivation of *Shaker* K_V channels.

Introduction

Voltage-gated potassium channels (K_V) play essential roles in a large variety of physiological processes: they contribute to the maintenance of the resting membrane potential of cells, influence the frequency and duration of action potentials in excitable tissues (Dodson and Forsythe, 2004), or regulate membrane potential-driven processes of non-excitable cells, such as antigen-dependent activation of T lymphocytes (Panyi et al., 2004; Varga et al., 2007). K_V channels are tetramers formed by four subunits containing a K^+-selective transmembrane pore. Each subunit consists of six transmembrane α-helical sequences (S1–S6) and intracellular N- and C-termini. S1–S4 helices form the voltage sensing domain (VSD) that moves from its resting position toward the extracellular compartment upon depolarization, as reported by gating current and voltage-clamp fluorometry measurements (Larsson et al., 1996; Baker et al., 1998; Bezanilla, 2000; Yellen, 2002). The pore domain (PD) is composed of the S5 and S6 helices and the pore loop connecting them contains the selectivity filter (SF) lined with carbonyl oxygen atoms that specifically interact with K^+ ions allowing rapid and selective conduction (Fig. 1 A; Doyle et al., 1998; Bernèche and Roux, 2001, 2003; Bernèche and Roux, 2001; Morais-Cabral et al., 2001; Bernèche and Roux, 2003). The activation gate (A-gate or lower gate) that controls access to the pore (Liu et al., 1997; Perozo et al., 1999; del Camino and Yellen, 2001) is formed by the crossing of the S6 helices of each of the four subunits at the intracellular end of the pore ("bundle crossing"). The A-gate is functionally coupled to the VSD (Lu et al., 2002).

K_V channels open in response to membrane depolarization allowing transmembrane K^+ fluxes (Liu et al., 1997). During sustained depolarization, most K_V channels enter a non-conducting inactivated state despite the continued presence of the activating stimulus. Inactivation proceeds by two distinct mechanisms, N- and C-type inactivation, which have been studied in detail and reviewed extensively (Kurata and Fedida, 2006). N-type inactivation is well described and occurs via the "ball-and-chain" mechanism (Hoshi et al., 1990; Zagotta et al., 1990), originally proposed for Na^+ channels (Bezanilla and Armstrong, 1977). In the absence of N-type inactivation, K_V channels are still able to inactivate through slow inactivation (Hoshi et al., 1991; Hoshi and Armstrong, 2013). The *Shaker*-IR channel lacking N-type inactivation is a dedicated model for examining the slow inactivation of K_V channels (Hoshi et al., 1990, 1991).

[1]Department of Biophysics and Cell Biology, Faculty of Medicine, University of Debrecen, Debrecen, Hungary; [2]Department of Physiology, University of Pennsylvania, Philadelphia, PA, USA.

Correspondence to Gyorgy Panyi: panyi@med.unideb.hu.

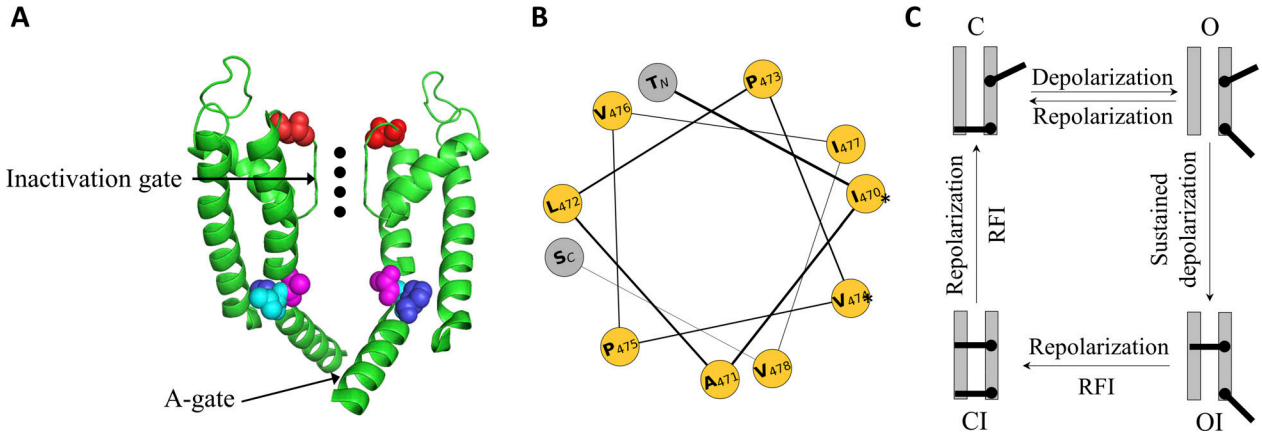

Figure 1. **Structure of the pore region and the four-state gating model of *Shaker*-IR. (A)** The structure of the pore domain of *Shaker*-IR channel (amino acid residues 390-489) in open conformation (PDB accession no. 7SIP) visualized by PyMol. The S5, S6, pore helix, and pore loop segments of two diagonally opposed subunits are shown as ribbon representations with front and rear subunits removed for clarity. Colored amino acids are T449 (red), A471 (purple), L472 (cyan), and 473 (blue). Potassium ions in the selectivity filter are illustrated by black dots. **(B)** Helical wheel projection of the pore domain (residues 469–479). Amino acid residues indicated by * at the right side of the helical wheel are facing the water-filled cavity in the open state. Color-coding indicates amino acid characteristics, yellow: hydrophobic; gray: polar. **(C)** Composite gating states and a simplified four-state gating model in which four major gating states can be distinguished depending on the status of the activation (lower) and inactivation (upper) gates. Among the closed (C), open (O), open-inactivated (OI), and closed-inactivated (CI) states, only the open state is conducting. Arrows indicate the theoretically existing transitions between these gating states. RFI represents recovery from slow inactivation.

Experimental, computational, and structural investigations suggest that slow inactivation is caused by molecular rearrangements at or near the SF region (here referred to as the inactivation gate or upper gate) that disrupt the interaction of the SF with K^+ ions. This creates a non-conducting permeation pathway (Zhou and MacKinnon, 2004; Cordero-Morales et al., 2006a; Cordero-Morales et al., 2006b; Cuello et al., 2010a; Cuello et al., 2010b; Cuello et al., 2017; Li et al., 2018; Karbat et al., 2019; Szanto et al., 2021). Two opposite modalities, pore dilation versus constriction, have been proposed to constitute the mechanism (Loboda et al., 2001; Cuello et al., 2010b; Hoshi and Armstrong, 2013; Li et al., 2018; Reddi et al., 2022; Tan et al., 2022). Moreover, several pieces of evidence support the idea that an extensive network of H_2O–H_2O and H_2O–protein hydrogen bond interactions behind SF are important for slow ("C-type") inactivation in the bacterial KcsA K^+ channel (Cordero-Morales et al., 2011; Ostmeyer et al., 2013; Pless et al., 2013; Cuello et al., 2017; Labro et al., 2018; Li et al., 2018) and in *Shaker*-like channels, as well (Karbat et al., 2019; Szanto et al., 2021).

According to the classic view, the combination of the A- and the inactivation-gates results in four composite gating states (Fig. 1 C). Left-to-right movement is the opening of the activation gate in response to membrane depolarization (C→O or CI→OI, where C and O represent the closed and open conformations of the activation gate, respectively, and I indicates a closed inactivation gate). Sustained depolarizations lead to slow inactivation (O→OI), and then, returning to sufficiently negative membrane potentials induces the closure of the A-gate (O→C and/or OI→CI). Using intramolecular Cd^{2+} bridges, we showed that locking the A-gate of the T449A/V476C *Shaker*-IR channel in the open state, the locked-open channel impedes recovery from inactivation, supporting that the OI→CI transition is a prerequisite for recovery from inactivation (Szanto et al., 2020).

Functional crosstalk between these two gates in *Shaker* K^+ channels is well-established: closure of the inactivation gate speeds opening and slows closing of the activation gate, i.e., stabilizing the gate in the open configuration (Panyi and Deutsch, 2006). Correlated movement of the activation gate at the bundle crossing (Fig. 1 A) with the movement of the slow inactivation gate has been observed directly by x-ray crystallography and EPR spectroscopy in the prokaryotic KcsA K^+ channel (Cuello et al., 2010a). Furthermore, recent high-resolution cryo-EM of *Shaker*-IR and its non-conducting, permanently inactivated W434F mutant shows that slow inactivation involves an unanticipated conformational rearrangement of the external pore leading to rearrangements of the P-loop and dilation of the ion selectivity filter (Tan et al., 2022). However, these static cryo-EM screenshots do not necessarily reveal the molecular mechanism by which the gates are coupled. Structural rearrangements were reported in the selectivity filter region but surprisingly not in S5 or S6. Either no S5/S6 rearrangements occur, or the limited image resolution or the inappropriate time-window preclude the detection of coupled S5/S6 events. Therefore, the nature of coupled molecular movements upon slow inactivation requires direct functional assays.

To investigate the molecular mechanism of this coupling, we engineered cysteine residues at strategic positions in S6 and determined their state-dependent modification kinetics by methanethiosulfonate (MTS) reagents using patch-clamp techniques (Sheng et al., 2001; Liu et al., 2006; Sheets and Hanck, 2007; Börjesson and Elinder, 2011; Schmid and Grissmer, 2011). Covalent modification by these reagents renders the channel non-conducting, thereby allowing the reaction to be monitored by measuring the ionic current. This approach provides information about the state-dependent accessibility of cysteines (Liu et al., 1997). For example, the accessibility of cysteine residues at

I470 and V474 in *Shaker* change upon inactivation: they are modified ~20-fold faster in the open state than in the inactivated state (Panyi and Deutsch, 2006; Panyi and Deutsch, 2007), consistent with an increased accessibility in the open state. This suggests allosteric communication between the gates mediated by conformational changes along S6 (Yifrach and MacKinnon, 2002; Sadovsky and Yifrach, 2007). We hypothesize (1) that inactivation produces a conformational change in S6, possibly a rotation about its longitudinal axis, and (2) this rearrangement contributes to the allosteric communication between the gates. Since 471–473 side chains face away from the cavity in the open state (Fig. 1. A and B) and are thus inaccessible, an S6 rearrangement or rotation predicts a concomitant change in cysteine accessibility at A471, L472, or P473 positions upon slow inactivation.

We tested this hypothesis by mutating residues A471, L472, and P473 to cysteines, one at a time, and determined MTS accessibility in the open, closed, and slow-inactivated state of the channel. As expected, none of the cysteines in positions 471, 472, and 473 can be modified either in the closed or the open state. In contrast, inactivation increases the accessibility of residue A471C and P473C for MTSEA (ethylammonium methanethiosulfonate) but not for the larger MTSET (ethyltrimethylammonium methanethiosulfonate). This state-dependent modification of the A471C and P473C mutants is consistent with S6 rotating around its own longitudinal axis upon inactivation, thereby mediating the coupling between the activation and inactivation gates.

Materials and methods

Cell culture

Human embryonic kidney cells transformed with SV40 large T antigen (*tsA201*) were grown in DMEM-high glucose medium supplemented with 10% FBS, 2 mM l-glutamine, 100 U/ml penicillin-G, and 100 µg/ml streptomycin (Invitrogen) at 37°C in a 5% CO_2 and 95% air humidified atmosphere. Cells were passaged twice per week following a 2–3 min incubation in PBS containing 0.2 g EDTA/liter (Invitrogen).

DNA clones and site-directed mutagenesis

Modified *Shaker*-IR channels in a GW1-CMV mammalian expression plasmid under the control of a highly expressing Kozak consensus promoter sequence (Kozak, 1991) were provided by R. Horn (Thomas Jefferson University, Philadelphia, PA; Ding and Horn, 2002). Mutations were introduced by PCR mutagenesis into *Shaker*-IR containing the deletion of residues 6 through 46 (Δ6–46) to eliminate the fast N-type inactivation (Hoshi et al., 1990). Moreover, all constructs include C301S and C308S point mutations to exclude possible modifications by MTS reagents of endogenous *Shaker* cysteines and accompanying functional effects. Point mutations expressing T449A/A471C, T449A/L472C, and T449A/P473C were introduced by using a site-directed mutagenesis kit (QuikChange; Stratagene). Calcium Phosphate Transfection Kit (Invitrogen) was used to co-transfect a GFP plasmid vector together with the *Shaker*-IR construct in a 1:10 molar ratio. As we could not detect any current from the homotetrameric T449A/P473C channels, a combination of homo- and heterotetramers were expressed by co-transfection of the T449 and T449A/P473C channel constructs at a molar ratio of 3:1. Heterotetramers are indicated as T449A/P473C//T449 throughout the text. Transfected cells were replated onto 35-mm polystyrene cell culture dishes (Cellstar, Greiner Bio-One) pretreated with poly-L-ornithine (Sigma-Aldrich) to improve cell adhesion for excising patches. Channels were expressed ~24–48 h after transfection. The GFP-positive transfectants were identified by a Nikon Eclipse TS100 fluorescence microscope using bandpass filters of 455–495 and 515–555 nm for excitation and emission, respectively. More than 70% of the GFP-positive cells expressed the co-transfected ion channels, as well.

Solutions and perfusion system

All ionic current experiments were performed with excised inside-out patches. The standard intracellular (bath) solution (ICS) contained (in mM) 105 KF, 35 KCl, 10 EGTA, and 10 HEPES titrated to pH 7.36–7.38 with KOH for a final concentration of ~160 mM K^+ and an osmolarity of 285–295 mOsm, while the standard extracellular (pipette-filling) solution (ECS) was (in mM) 150 NaCl, 5 KCl, 1.5 $CaCl_2$, 1 $MgCl_2$, and 10 HEPES at pH 7.36–7.38 with NaOH and an osmolarity of ~290 mOsm. For experiments using 50 mM K^+, the composition of the 50 K^+-ICS was (in mM) 50 KF, 55 NaF, 35 NaCl, 10 HEPES, and 10 EGTA. MTSET and MTSEA (Toronto Research Corp.) solutions were made fresh in ICS from 100 mM stocks in water stored at −80°C. MTS reagents were freshly diluted into the ICS from stocks and loaded immediately into the perfusion system ~1 min before the start of MTS application. Freshly diluted MTS reagents were loaded into the perfusion apparatus every ~10 min.

A Warner Instruments SF-77 A Perfusion Fast-Step system with three-barrel square glass (700 µM internal diameter) was used for rapid solution exchange. The patches were perfused with solutions at a rate of 0.5 ml/min. Fig. S1 shows the calibration of the solution exchange. The solution exchange is determined by a mechanical/electrical delay (d) followed by a rapid exponential decay characterized by an exchange time constant (τ_e). The medians of d and τ_e were 24.9 ± 0.7 and 10.9 ± 1.0 ms, respectively (n = 30). Based on the kinetics, complete solution exchange was achieved in ~4 × τ_e = 40 ms.

Electrophysiology

Standard methods (Hamill et al., 1981) were used to record currents in inside-out patches. The direction of K^+ currents and the voltage protocols are presented according to general conventions. Typical current amplitudes were 300–3,000 pA at +50 mV test potential, thereby allowing the recording of macroscopic currents. Micropipettes were pulled in four stages by using a Flaming Brown automatic pipette puller (Sutter Instruments) from Borosilicate Standard Wall with Filament aluminum-silicate glass (Harvard Apparatus Co). Tip diameters ranged from 0.5 to 1 µm and heat polish gave tip resistances of 2–8 MΩ. All measurements were carried out using an Axopatch 200B amplifier connected to a personal computer using Axon Digidata 1320 data acquisition hardware (Molecular Devices Inc.). In general, the holding potential was −120 mV. Records

were discarded when the leak at the holding potential was >10% of the peak current at the test potential. Experiments were done at room temperature ranging between 20 and 24°C. Data were analyzed using the pClamp9 software package (Molecular Devices Inc.) and GraphPad Prism 8 (GraphPad). Before analysis, current traces were digitally filtered with a three-point boxcar smoothing filter. Reported errors are SEM.

Data analysis

To determine the essential biophysical properties of the investigated mutant channels, we studied the kinetics of activation and inactivation, the voltage dependence of steady-state activation and inactivation, and the kinetics of recovery from slow inactivation. To study activation kinetics, cells were depolarized to +50 mV for 15 ms from a holding potential of –120 mV every 15 s. K^+ current traces were fitted with a single exponential function rising to the maximum according to the Hodgkin-Huxley n^4 model $\left\{I(t) = I_a \times [1 - \exp(-t/\tau_{act})]^4 + C\right\}$, where I_a is the amplitude of the activating curve component, τ_{act} is the activation time constant of the current, and C is the amplitude of the non-activating current component. The τ_{act} for a particular cell was determined as the average of τ_{act} values obtained for three to four depolarizing pulses repeated every 15 s. We recorded n = 22–24 cells of a given *Shaker*-IR construct, and the average of τ_{act} was used to demonstrate the activation kinetics. To study channel inactivation of T449A/A471C and T449A/L472C, 1-s-long depolarizing pulses to +50 mV were applied from a holding potential of –120 mV every 60 s. The rapid activation of the current is followed by a decay corresponding to slow inactivation. A single exponential function $[I(t) = I_0 \times exp(-t/\tau_i) + C]$, where I_0 is the amplitude of the inactivating component of the current, τ_i is the inactivation time constant for the given *Shaker*-IR construct, and C is the steady-state current at the end of the depolarizing pulse, was fitted to the decaying part of the current traces to obtain the time constant (τ_i) characterizing the inactivation kinetics. In contrast, traces recorded from the T449A/P473C//T449 heterotetramers clearly showed a fast and a slow component of the decay, therefore, the falling phase of the currents was fit by the sum of two exponential terms, $[I(t) = A_f exp(-t/\tau_{i,f}) + A_s exp(-t/\tau_{i,s}) + C]$ giving $\tau_{i,f}$ and $\tau_{i,s}$. To determine the voltage dependence of steady-state activation of the current, the cells were held at –100 mV and depolarized to test potentials ranging from –80 to +70 mV in 10-mV increments every 60 s. Peak conductance (G(V)) at each test potential was calculated using $G(V) = I_{peak}/(E_m - E_K)$, where I_{peak} is the peak current at a test potential of E_m and E_K is the reversal potential of K^+ (–86.9 mV, based on the Nernst equation). The G(V) values were then normalized for the maximum conductance (G/G_0) and plotted as a function of test potential along with the best-fit Boltzmann function $\{G/G_0 = 1/[1 + exp[-(V - V_{\S})/s]]\}$, where G/G_0 is the normalized conductance, V is the test potential, $V_{½}$ is the midpoint voltage, and s is the slope factor of the function. To describe the voltage dependence of steady-state inactivation, the fraction of noninactivated channels at each test potential was calculated as I/I_{-120}, where I is the peak current evoked by the depolarization from a given prepulse potential and I_{-120} is the peak current evoked by identical depolarization from the holding potential of –120 mV. $V_{1/2}$ and k were determined by fitting a Boltzmann function to the data points. To study the kinetics of recovery from inactivation, pairs of depolarizing pulses were applied from the holding potential of –120 to +50 mV for 400 ms. The duration of the first step was used to inactivate channels and measure the initial peak current amplitude (I_1). After a recovery period, defined as the interpulse interval (ipi) at –120 mV, the second identical voltage step was applied and the peak amplitude of the recovered current (I_2) was measured. The ipi at –120 mV varied between 1.8 and 60 s. The fractional recovery (FR) at a given ipi was calculated as $FR = (I_2 - I_{ss1})/(I_1 - I_{ss1})$, where I_2 and I_1 are the peak currents of the second and first pulse, respectively, and I_{ss1} is the steady-state current at the end of the first depolarizing pulse. The FR versus ipi plot was fit with an exponential function rise to a maximum containing a single term, $FR(t) = 1 - exp(-t/\tau_{rec})$ to give the time constant of recovery from inactivation, τ_{rec}. Prior to analysis, current traces were corrected for ohmic leak. Nonlinear least square fits were done using the Levenberg–Marquardt algorithm. The number of experiments on different cells (n) involved in the given analysis is shown in the text. Data are expressed as mean ± SEM.

Cysteine modification assay

Inside-out patches were depolarized from a holding potential of –120 to +50 mV for the time required to achieve the open or fully inactivated state of the channels. Pulse protocols were repeated three to four times in the absence of the MTS reagents to verify the stability of the peak currents. Patches showing >10% run-down in peak current were discarded. MTSEA (2 mM) or MTSET (0.2 mM) were applied for the indicated duration (L) either at the hyperpolarized holding potential (e.g., –120 mV) or during depolarization, depending on the state of the channel being probed. Voltage protocols used for state-dependent accessibility assays were repeated 8–12 times in the presence of the modifying agents to monitor their effect. The normalized current was calculated as $I(t)/I_0$, where I_0 is the peak current at +50 mV prior to application of the MTS reagent and I(t) is the peak current at cumulative MTS modification time t. A single exponential function was fit to the normalized current-cumulative MTS modification time graph: $I(t) = I_0 \times exp(-t/\tau_{mod}) + C$, where τ_{mod} is the modification time constant and C is the steady-state current at the equilibrium current reduction. The modification rate constant (k_{mod}) was determined as $1/(\tau_{mod} \times [MTS])$, where [MTS] is the molar concentration of the MTS reagent. Nonlinear least square fits were done using the Levenberg–Marquardt algorithm. Data are expressed as mean ± SEM.

Online supplemental material

Fig. S1 shows the characterization of the solution exchange kinetics of the perfusion system. Fig. S2 shows the biophysical characterization of the T449A/L472C *Shaker*-IR channel K^+ currents. Fig. S3 shows the biophysical characterization of the heteromeric T449A/P473C//T449 *Shaker*-IR channel K^+ currents. Fig. S4 shows the extended application (300 ms) of MTSEA to the T449A/A471C *Shaker*-IR channel in the open state.

Results

Biophysical characterization of the mutant channels

To study the accessibility of S6 residues 471–473, we introduced these cysteines, one at a time, into a well-established *Shaker*-IR background (Yellen, 2002). This background construct has an N-terminal deletion (Δ6–46) to eliminate fast N-type inactivation and C301S and C308S to obviate modification of native cysteines. In addition, we replaced the native T449 at the external mouth of the channel with alanine to produce a slow inactivation rate compatible with the planned experiments. Wild-type *Shaker*-IR inactivates slowly (τ_i ~1,000 ms), whereas the T449A mutant inactivates considerably faster (τ_i ~100 ms; López-Barneo et al., 1993; Szanto et al., 2021), which is ideal for cysteine modification measurements (see below; Panyi and Deutsch, 2006; Panyi and Deutsch, 2007). Thus, we engineered T449A/A471C, T449A/L472C, and T449A/P473C mutants in the *Shaker*-IR background. The first two mutants expressed K^+ currents in tsA201 cells (Fig. 2 A and Fig. S2 A), whereas the T449A/P473C mutant did not, similar to other *Shaker*-IR channels mutated at residue P473 (Hackos et al., 2002) or $K_V1.2$ channels mutated at the analogous position (Choe and Grabe, 2009). However, functional heterotetrameric channels were produced by coexpression of T449A/P473C and the T449 WT *Shaker*-IR background that has a proline at 473, referred to as T449A/P473C//T449 (see below, Figs. 3, 4, 5, and 6; and Fig. S3). Although the random subunit stoichiometry results in a heterogeneous channel population, this construct enabled us to perform the accessibility experiments.

First, we characterized the electrophysiological properties of the mutant channels in inside-out patches to optimize our pulse sequence voltage protocols and the timing of the application of MTS reagents. Figs. 2, S2, and S3 show the essential gating parameters of all *Shaker*-IR constructs including the voltage dependence of activation (peak conductance–voltage, or G–V, curve), the voltage dependence of steady-state inactivation, the kinetics of activation, slow inactivation, and recovery from inactivation. The G–V curve was calculated from the current–voltage relationship, which was obtained with a series of 1-s-long depolarizing pulses ranging from −80 mV to +70 mV every 60 s (Fig. 2 A, Fig. S2 A, and Fig. S3 A), and the voltage dependence of the conductance was determined (Fig. 2 B) by fitting a Boltzmann function to the normalized conductance (G/G_0)-test potential relationships to give the midpoint voltage ($V_{1/2}$) and slope factor (s). Although the mutations produce a range of midpoint voltages (see Table 1 for $V_{1/2}$ and s values, similar to other *Shaker* mutations that change $V_{1/2}$, s, or both; Hackos et al., 2002; Soler-Llavina et al., 2006), each channel was fully activated by depolarizing pulses to +50 mV. The activation time constants of the currents are similar for all constructs (0.3–0.7 ms) in response to a depolarization to +50 mV. Pulses of 5 ms duration were sufficient to activate all channels. Time constants of slow inactivation (Fig. 2 C, Fig. S2 C, and Fig. S3 C) were obtained by fitting decaying exponential functions to the current traces recorded during long (1.0–3.0 s) depolarizing pulses. Traces from T449A/A471C and T449A/L472C were well fit by single exponential functions, but traces recorded from the T449A/P473C//T449 heterotetramers contained a fast and a slow component of the decay (see Table 1 for the time constants of inactivation, τ_i). Nevertheless, during depolarizing pulses of a 3-s duration, the current amplitudes decayed to <15% of the peak values, consistent with the majority (>85%) of the channels having entered the slow inactivated state. To assess the voltage dependence of steady-state inactivation (h_∞), we applied 3-s-prepulse potentials from −110 to −20 mV in 10-mV increments before stepping the test potential to +50 mV for 5 ms. The fraction of noninactivated channels at each voltage was calculated as I/I_{-120} and plotted as a function of prepulse potential (see Materials and methods). The voltage dependence of steady-state inactivation was characterized by $V_{1/2}$ and a slope factor determined from Boltzmann fits for I/I_{-120}–prepulse potential relationships (Fig. 2 D, Fig. S2 D, and Fig. S3 D; see Table 1 for $V_{1/2}$ and s values). The kinetics of recovery from inactivation were studied using pairs of depolarizing pulses delivered from the holding potential of −120 to +50 mV for 400 ms and varying the ipi at −120 mV. The FR versus ipi plot was fit with a single-exponential function regardless of the channel mutant to give the time constant of recovery from inactivation (τ_{rec}; Fig. 2 F, Fig. S2 F, and Fig. S3 F; see Table 1 for the time constants). Recovery time constants for the T449A/A471C, T449A/L472C, and T449A/P473C//T449 channels were 9.4 ± 0.8 (n = 5), 4.4 ± 0.7 (n = 5), and 1.8 ± 0.2 (n = 5) s, respectively. Full recovery from inactivation was achieved by holding the patch at −120 mV for a duration of at least five times longer than the time constant for recovery from inactivation for a given construct.

The gating parameters (Table 1) were used to define the voltage range (more than +50 mV) where currents quickly and fully activate, and slow inactivation can be studied in isolation. Moreover, all of these data allowed us to define a sufficiently negative holding potential (−120 mV) and interepisode time (>45 s) that ensured full recovery of the channels from inactivation and that all channels are in the closed state at the holding potential. Altogether, the kinetic parameters of the mutant channels, i.e., an inactivation time constant of a few tens of milliseconds and a recovery time constant of a few seconds, rendered them ideal for MTS modification measurements, whose aim is to determine whether inactivation alters the solvent accessibility of S6 residues, thereby implicating a mechanism by which the gates are coupled.

Cysteine accessibility in the closed and open states of the channels

A previous cysteine scan of the S6 transmembrane segment between the selectivity filter and the bundle crossing (positions 470–477) showed that these residues are not accessible to MTS reagents when the activation gate is closed, but residues at positions 470 and 474–477 were readily modified in the open state (Liu et al., 1997). However, no significant modification of residues 471–473 was detected in the open state. We first confirmed these findings in our system before examining the accessibility of these residues with MTS reagents in the slow-inactivated state. The accessibility of the introduced cysteine residues was tested using the neutral/partially positively charged MTSEA (3.6 Å) and the larger and permanently positively charged MTSET (5.8 Å). These differences in size allowed us to explore the

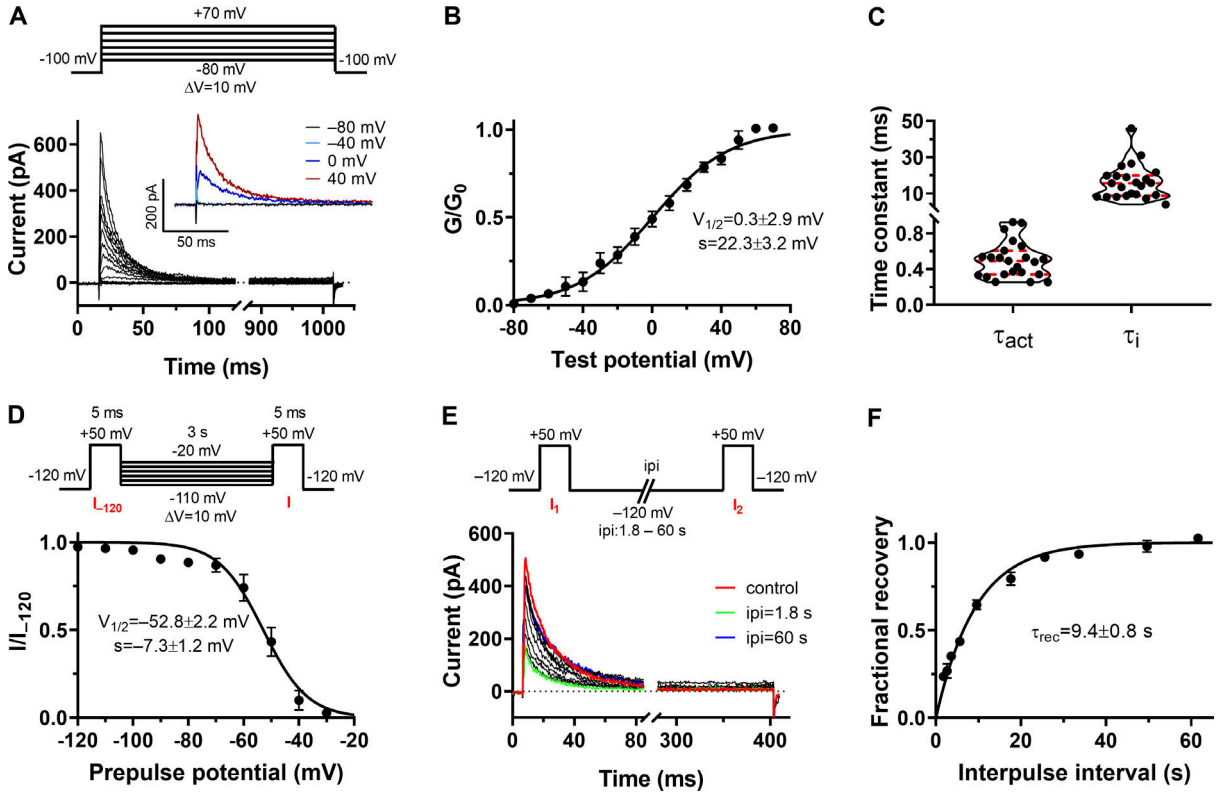

Figure 2. **Characterization of K⁺ currents of the T449A/A471C *Shaker*-IR mutant. (A)** Ionic currents of T449A/A471C channel expressed in tsA201 cells. The inside-out patch was held at −100 mV and depolarized to test potentials ranging from −80 to +70 mV in steps of 10 mV every 60 s. The duration of the depolarizing pulses was 1 s. Inset shows K^+ currents evoked by the depolarizing pulses to the indicated membrane potentials. **(B)** Normalized G–V data (see Materials and methods) were obtained from the peak currents (I_{peak}) at the test potential of E_m and the K^+ reversal potential (E_K) using $G(V) = I_{peak}/(E_m - E_K)$. The G(V) values were normalized for the maximum conductance (G/G_0) for six independent measurements, averaged, and then plotted as a function of test potential. The superimposed solid line is the best-fit Boltzmann function to the averaged data points. The mean values ± SEM of the midpoint ($V_{1/2}$) and slope factor (s) are shown. **(C)** Activation kinetics were studied using 5-ms-long depolarizing pulse from a holding potential of −120 to +50 mV. Current traces were fitted using the Hodgkin-Huxley n^4-model, and the activation time constant (τ_{act}) was used to describe the activation kinetics. The inactivation time constant (τ_i) of the current at +50 mV was determined by fitting a single exponential function to the decaying part of the currents shown in Fig. 2 A. Violin plots show Q1, median, and Q3 for n = 23 independent experiments, and symbols indicate individual data points. **(D)** Voltage dependence of steady-state inactivation was measured in inside-out patches. The voltage protocol (top) consisted of a brief (5 ms) step from a holding potential of −120 to +50 mV to record I_{-120}. The patch was then held between −110 and −20 mV in steps of 10 mV for 3 s, and then a short (5-ms) test pulse to +50 mV was applied to obtain I. After each pulse pair, the patches were held at −120 mV holding potential for 45 s. The fraction of noninactivated channels (I/I_{-120}) at each prepulse potential was averaged for n = 5 cells (biological replicates) and plotted as a function of prepulse potential. The superimposed solid line shows the best-fit Boltzmann function to the averaged data points. The mean values ± SEM of the midpoint ($V_{1/2}$) and slope factor (s) are shown. **(E)** Kinetics of recovery from inactivation were determined using pairs of depolarizing pulses from the holding potential of −120 to +50 mV for 400 ms. The ipi at −120 mV varied between 1.8 and 60 s. Current traces highlighted in red, green, and blue were recorded during the second pulse with ipi of 1.8 and 60 s and control, prior to the start of the pulse pairs, respectively. **(F)** FR was calculated as $I_2 - I_{ss1}/I_1 - I_{ss1}$, where I_2 and I_1 are the peak currents during the second and first pulse, respectively, and I_{ss1} is the current at the end of the first depolarization. The FR averaged for n = 5 cells versus ipi plot was fit with an exponential rise to maximum function to give the time constant of recovery from inactivation (τ_{rec}). Data are given as mean ± SEM (n = 5), n values are biological replicates in all panels.

spatial alterations in the molecular microenvironment of S6 at the water-filled cavity upon inactivation. The closed state is characterized by an open inactivation gate and closed activation gate, as shown by pictograms in Fig. 3. The heterotetrameric T449A/P473C//T449 channels are indicated by a combination of a white- and grey-filled rectangle in the pictograms throughout the text. The accessibility of the closed state was studied as follows: the channels were exposed to 2 mM MTSEA or 0.2 mM MTSET for 500 ms (L = 500 ms, see Materials and methods) while being held closed at −120 mV. After a complete wash-out of the reagents by perfusing the patch with MTS-free ICS for 600 ms (lag time), the effect of the MTS application on the peak K^+ currents was assessed by brief depolarizing pulses to +50 mV. A step to +50 mV ensures that all channels open quickly since the opening probability is maximal at this voltage (Fig. 2 B; Fig. S2 B and Fig. S3 B). These steps were repeated every 15 s. As shown in Fig. 3, neither MTSEA nor MTSET caused a significant current reduction in any of the mutant channels confirming the inaccessibility of these pore-lining residues in a channel with a closed activation gate. The normalized currents after 3.5 s cumulative perfusion with MTSEA and MTSET were 0.935 ± 0.002 (n = 5) and 0.924 ± 0.043 (n = 4) for T449A/A471C; 0.954 ± 0.014 (n = 4) and 0.947 ± 0.025 (n = 4) for T449A/L472C; and 0.939 ± 0.024 (n = 5) and 0.947 ± 0.036 (n = 4) for T449A/P473C//T449, respectively.

In the open state (state O in Fig. 1 C), both the activation gate and the inactivation gate are in their conducting conformation

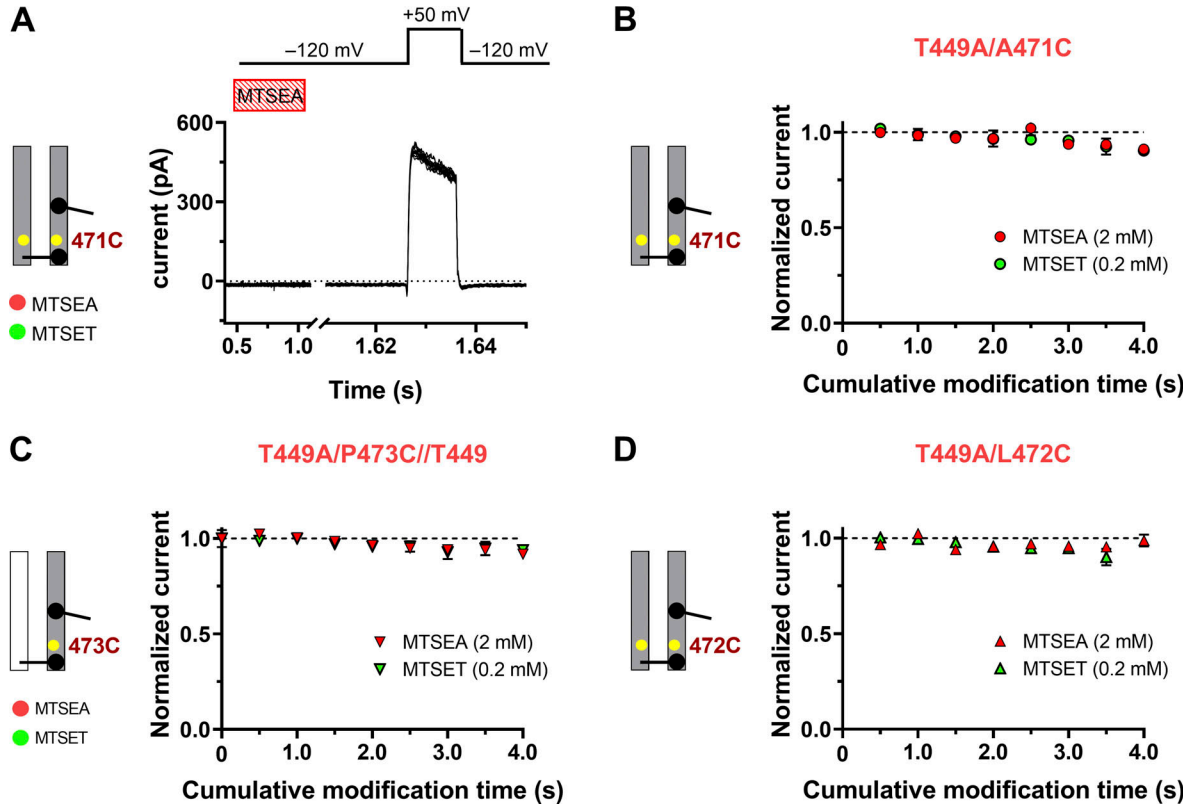

Figure 3. **Application of MTS reagents to the closed channels.** The pictograms on the left indicate the status of the activation (lower) and inactivation (upper) gates. **(A)** The K^+ current was measured from a voltage-clamped inside-out patch containing T449A/A471C channels. Channels were held closed at −120 mV, and their activity was monitored using brief depolarizing pulses to +50 mV every 15 s to measure the K^+ current. The patch was exposed for L = 500 ms to 2 mM MTSEA (red hatched bar, MTSEA) and then washed out before the test pulse (lag time = 600 ms). **(B–D)** Normalized current as a function of cumulative modification time of the MTS reagents: 2 mM MTSEA (red symbols) or 0.2 mM MTSET (green symbols) in the ICS for T449A/A471C (B), T449A/P473C//T449 (C), and T449A/L472C (D). Data were obtained using the protocol explained in A. Filled circles, T449A/A471C; triangle up, T449A/L472C; triangle down, T449A/P473C//T449. Mean ± SEM for at least n = 4 (biological replicate) experiments are shown throughout the figure.

(see cartoons in Fig. 4). The inside-out patches were perfused with the MTS-free, KF-based ICS solution during the interpulse holding potential of −120 mV. Perfusion with MTS reagents started 200 ms prior to the depolarizing pulse that ensures solution exchange considering the delays in the perfusion system (Fig. S1) and the MTS reagent (2 mM MTSEA or 0.2 mM MTSET) was present during the entire duration (5 or 10 ms) the channels were held open. It was necessary to confine the duration of the depolarizing pulses to 5–10 ms to isolate the open conformation of both gates and avoid the entry of channels into the inactivated state. The voltage and MTS application protocol was repeated every 15 s. The peak currents for each pulse (I(t)) were normalized to the peak current of the last pulse in the absence of the MTS reagent (I_0) and plotted as a function of the cumulative modification time as shown in Fig. 4. Our results confirmed previous findings that cysteines at positions 471–473 are not modified by MTS reagents even in the open state of the channel when the A-gate is open. The normalized currents after 12 consecutive depolarizing pulses in MTSEA and MTSET were 0.982 ± 0.019 (n = 5) and 0.936 ± 0.06 (n = 6) for T449A/A471C; 0.936 ± 0.034 (n = 6) and 0.947 ± 0.057 (n = 7) for T449A/L472C; and 0.949 ± 0.041 (n = 6) and 0.951 ± 0.012 (n = 3) for T449A/P473C//T449, respectively. Even when the cumulative MTSEA exposure of the T449A/A471C open state is as long as 300 ms, there is no reduction in current (the normalized current after 60 consecutive depolarizing pulses in MTSEA was 0.935 ± 0.018 [n = 6]; Fig. S4), thereby suggesting a lower probability that slow open-state modification will contaminate our measurements of modification of the inactivated state.

Cysteine accessibility in the inactivated channel

I470C and V474C (see Panyi and Deutsch, 2006), but not 471–473C, are accessible to MTS reagents in the open state. This may be explained by their position on the S6 helix where side chains of 471–473 face away from the aqueous cavity pathway in the open state (Fig. 1, A and B). However, cysteines in these positions may rotate to become solvent accessible during the conformational rearrangements associated with slow inactivation. We tested this hypothesis by applying the MTS reagents during a period when the majority of the channels are in the inactivated state (Figs. 5 and 6). The A471C and L472C mutants with fast inactivation were completely inactivated by depolarizing pulses of 1-s duration. Application of the MTS reagents was started 300 ms after the start of the depolarization and lasted for L = 500 ms. Fig. 5, A and B, shows that intracellular application of 2 mM MTSEA to inactivated A471C channels

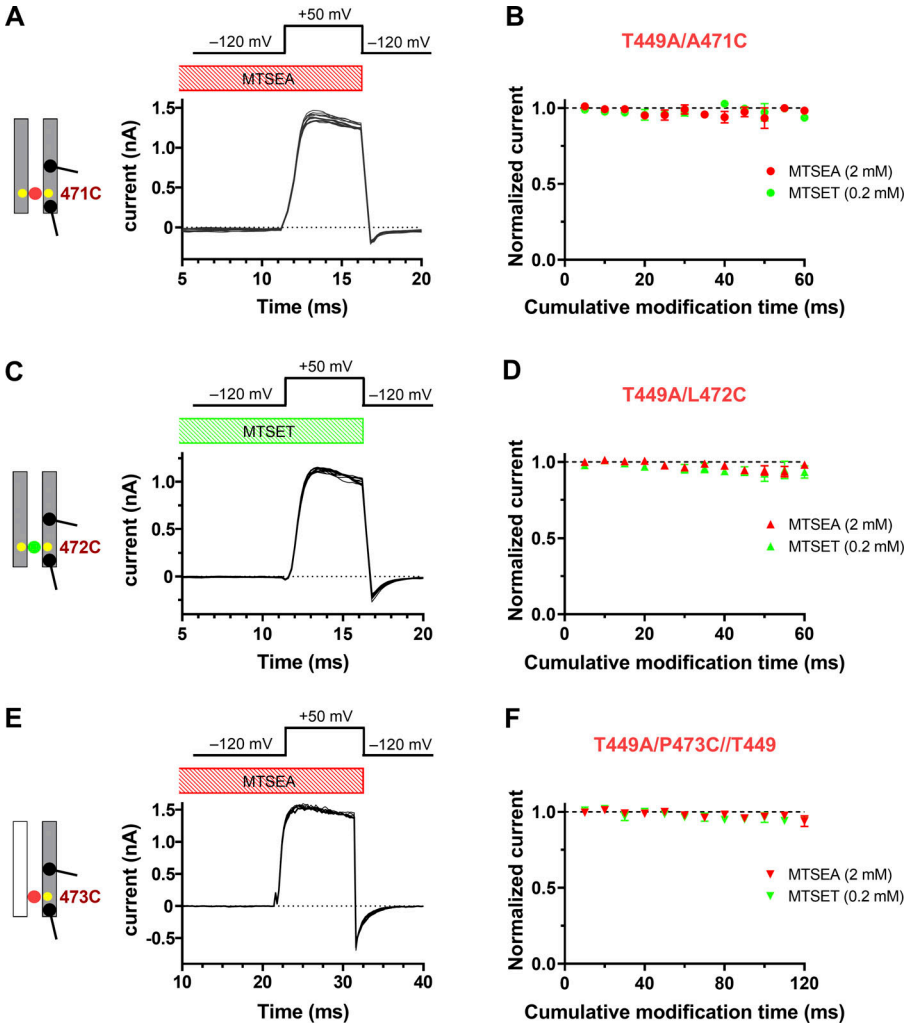

Figure 4. **Application of MTS reagents to the open channels. (A, C, and E)** The pictograms on the left indicate the status of the activation (lower) and inactivation (upper) gates. Depolarizing pulse durations were 5 ms for T449A/A471C (A, 471C) and for T449A/L472C (C, 472C) or 10-ms-long for the T449A/P473C//T449 heteromeric construct (E, 473C). Depolarizing pulses were delivered from the holding potential of –120 to +50 mV every 15 s in the presence of 2 mM MTSEA (red symbols) or 0.2 mM MTSET (green symbols) in the ICS. The perfusion with MTS reagents started 200 ms prior to the application of and during the depolarizing pulse. The patches were perfused with MTS-free ICS (see Materials and methods) for the duration of the interpulse holding potential. **(B, D, and F)** Peak currents for each pulse in the presence of MTS (I(t)) were normalized to the last peak current prior to MTS application (I_0) and plotted as a function of cumulative modification time (t). Mean ± SEM for at least n = 3 (biological replicates) experiments are shown throughout the figure.

irreversibly reduced the current with a time constant of 1.24 ± 0.12 s (n = 13). The modification rate constant (k_{mod}) is calculated as $1/(\tau_{mod} \times [MTSEA])$, where [MTSEA] is the molar concentration of MTSEA. The average of 13 replicate experiments yields a k_{mod} for the inactivated state of 485 ± 82 $M^{-1}s^{-1}$. The modification rate of T449A/A471C channels in the OI state by MTSEA (485 $M^{-1}s^{-1}$) is slightly slower than that of the T449A/I470C construct (660 $M^{-1}s^{-1}$; Panyi and Deutsch, 2007) but substantially slower than the modification of V474C (~18,000 $M^{-1}s^{-1}$; Panyi and Deutsch, 2007). However, MTSET at 0.2 mM caused no current reduction under the same conditions (Fig. 5, C and D). L472C was not affected by either reagent (Fig. 6, A and B).

Due to the slow biphasic inactivation of T449A/P473C//T449, we used longer depolarizing pulses of 3-s duration and started MTS application 2 s after the start of the depolarizing pulse, and the reagents were applied for an extended duration of L = 800 ms. In the case of mutant P473C, current from heterotetramer channels comprised of T449A/P473C and T449/P473 subunits was reduced by MTSEA, but not MTSET (Fig. 6, C–F). The kinetics and the modification rate of P473C in the OI state could not be mathematically determined since the normalized peak current versus cumulative modification time relationship does not follow a single exponential, but rather, a sigmoidal curve. These complex kinetics may originate from the weight of each channel type having 1, 2, or 3 of the T449A/P473C subunits present in the heterotetramer and consequently, an undetermined number of cysteines to be modified to result in current loss (Yellen et al., 1994). This uncertainty is also reflected in the larger error bars in the normalized current-cumulative modification time graph in Fig. 6 D. In contrast, the homotetrameric wild-type (T449/P473) channel was not modified by MTSEA (Fig. 6 D, empty circles), indicating specific interaction of the reagent with the engineered P473 cysteine in the heterotetramer. Regardless, qualitatively, the P473C residues are modified by MTSEA in the OI state over a comparable cumulative modification time range (~8 s) as A471C (~4 s).

Discussion

In this study, we investigated the state-dependent accessibility of cysteine residues in the S6 helix of the voltage-gated *Shaker* K^+ channel to gain insight into the molecular mechanism of coupling between the A-gate and the slow-inactivation gate of the channel (Panyi and Deutsch, 2006, 2007). The communication between the two gates is bidirectional: the closed slow-inactivation gate influences the rate of A-gate opening and

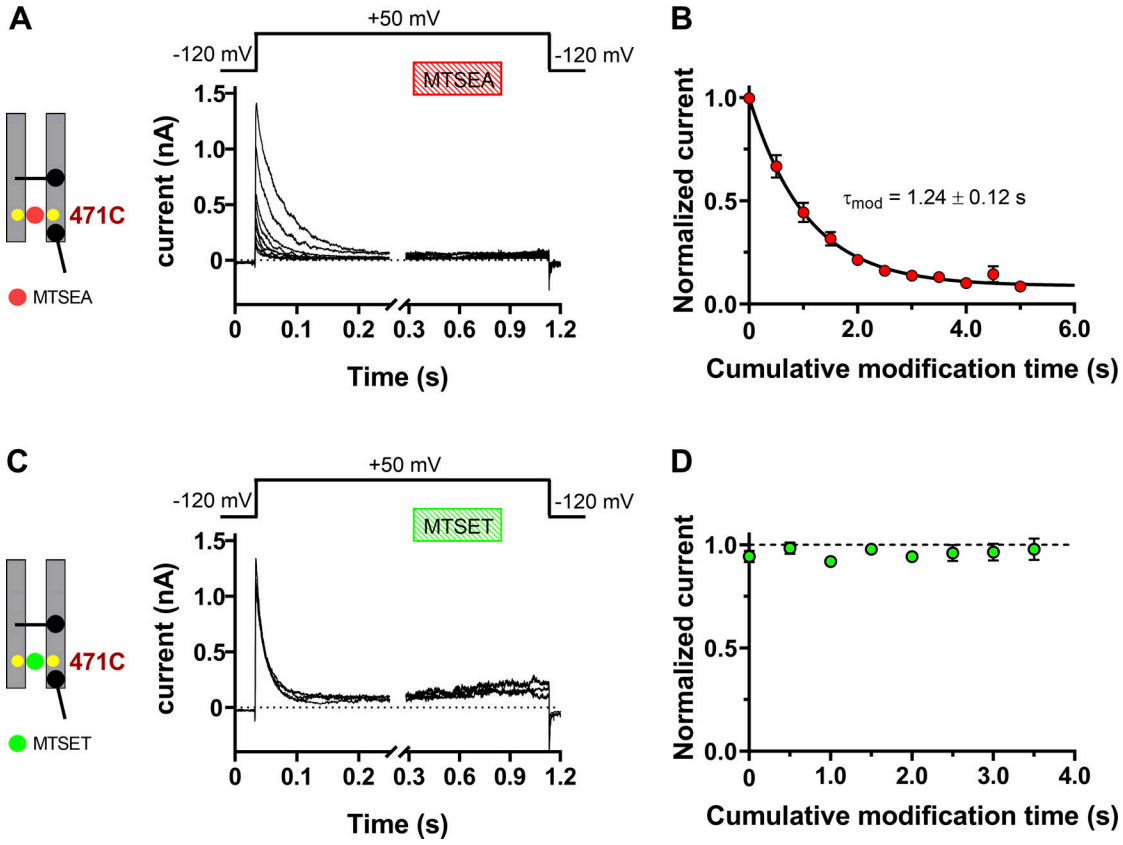

Figure 5. **Application of MTS reagents to the inactivated T449A/A471C channels.** The pictograms on the left indicate the status of the activation (lower) and inactivation (upper) gates. Patches were repeatedly depolarized from a holding potential of −120 mV using the pulse protocols shown above the corresponding raw current traces. The timing and the duration of the MTS pulses in ICS are indicated by the hatched bars. **(A and B)** 2 mM MTSEA modifies T449A/A471C channels. **(A)** 1.0-s-long depolarizing pulses were applied every 60 s and perfusion with 2 mM MTSEA (duration (L) = 500 ms) was initiated 300 ms after the start of the depolarization. **(B)** Peak currents for each pulse (I(t)) were normalized to the peak current of the last pulse prior to MTS application (I_0), averaged, and plotted as a function of cumulative modification time (t). The superimposed line is the best fit for a single exponential function. The reciprocal of the time constant is divided by the [MTSEA] to give a second-order rate constant of 485 ± 82 $M^{-1}s^{-1}$ (n = 13, biological replicates). **(C)** Same experiment as in A, except 0.2 mM MTSET was applied for L = 500 ms. Mean ± SEM for at least n = 3 (biological replicates) experiments are shown throughout the figure.

closure (Panyi and Deutsch, 2006) whereas A-gate opening precedes the closure of the inactivation gate. Moreover, recovery from inactivation requires A-gate closure (Szanto et al., 2020). The molecular rearrangements in the selectivity filter associated with slow inactivation and the consequent changes in the K^+ occupancy of the K^+ coordination sites controlling slow inactivation have already been proposed by x-ray crystallography and MD simulations in KcsA (Zhou and MacKinnon, 2004; Cuello et al., 2010b; Cuello et al., 2017; Li et al., 2018; Renart et al., 2019) and K_V1.2 (Reddi et al., 2022), and more recently in *Shaker* and K_V1.3 using cryo–EM (Ong et al., 2022; Tan et al., 2022). Despite these characterizations of the inactivated state of *Shaker*, several questions remain unanswered.

For example, how are filter conformational changes coupled to structural changes in the activation gate? What is the molecular mechanism of the coupling between the activation and inactivation gate? To address these issues and the status of the S6 helix upon slow inactivation, we used state-dependent modification assays as a tool, similar to that first used by Yellen and coworkers, to locate the activation gate in the lower portion of S6 (Liu et al., 1997; del Camino and Yellen, 2001). We found that slow inactivation increases the accessibility of S6 residues that are buried in the open state of *Shaker*-IR channels. This is consistent with the idea that communication of the gates is mediated by rearrangements in the S6 segment, as discussed below.

We have studied the kinetics of slow inactivation in three *Shaker*-IR mutants having inactivation time constants ranging from ∼15 to ∼600 ms. The current activates quickly (within 1 ms) in all three mutants (471–473) and the inactivation kinetics are fast enough to conduct the experiments on a reasonable time scale. All three mutants contain an alanine mutation at position T449 that has already been confirmed to modify rather than disrupt slow inactivation (López-Barneo et al., 1993; Cordero-Morales et al., 2006b; Hoshi and Armstrong, 2013; Cuello et al., 2017; Szanto et al., 2021). These indicate that the mutants utilized in our study are suitable to study slow inactivation. The mutants modify the inactivation rate rather than directly alter the conformational changes in the selectivity filter that underlie slow inactivation (Tan et al., 2022).

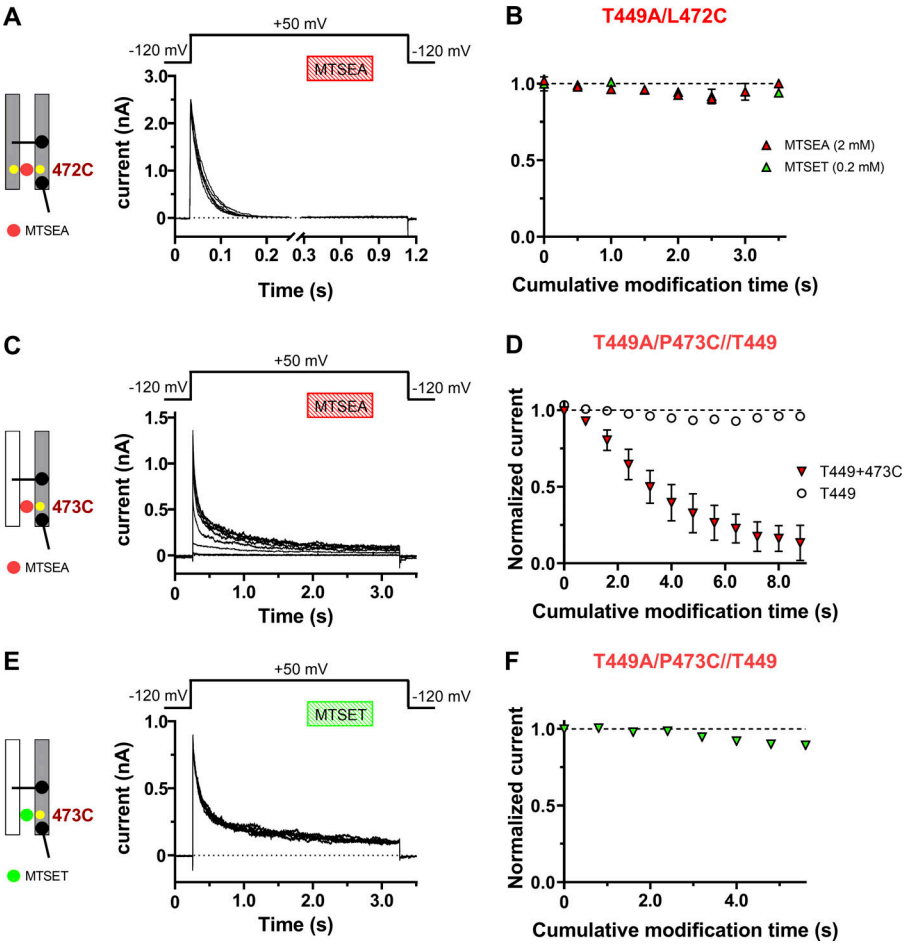

Figure 6. **Application of MTS reagents to the inactivated T449A/L472C, T449A/P473C//T449, and T449 *Shaker*-IR channels.** The pictograms on the left indicate the status of the activation (lower) and inactivation (upper) gates. Inside-out patches were repeatedly depolarized from a holding potential of −120 to +50 mV to elicit K^+ current through the channels. The timing and the duration of the MTS exposure (in ICS) to the inactivated channels are indicated by the hatched bars. Peak currents for each pulse (I(t)) were normalized to the peak current of the last pulse prior to MTS application (I_0), averaged, and plotted as a function of cumulative modification time (*t*). The abscissa shows the cumulative exposure to MTS reagents throughout the figure. **(A and B)** 1-s-long depolarizing pulses were applied for T449A/L472C channels. MTS application was initiated 300 ms after the start of the depolarizing pulse (L = 500 ms). Normalized peak currents upon repeated treatment with 0.2 mM MTSET (green symbols) or 2 mM MTSEA (red symbols) are shown. **(C and D)** The modification of the inactivated T449A/P473C//T449 heteromeric channels was determined during repeated 3.0 s depolarizations to +50 mV. A decrease of the peak currents occurs upon the application of 2 mM MTSEA (L = 1,000 ms, red down triangles). The wild-type (449T/P473) *Shaker*-IR channel was not modified with 2 mM MTSEA (open circles). **(E and F)** Same experiments as in C and D, except 0.2 mM MTSET was applied to the inactivated T449A/P473C//T449 channels for L = 800 ms. Mean ± SEM for at least *n* = 3 (biological replicates) experiments are shown throughout the figure.

The state-dependent cysteine accessibility technique is an excellent probe to study conformational changes occurring within the K^+ channel pore, such as those that are associated with inactivation (Yellen et al., 1994; Liu et al., 1996; Panyi and Deutsch, 2006, 2007) and those underlying the reduced intracellular TEA^+ affinity of the inactivated *Shaker*-IR channels (Panyi and Deutsch, 2007). This method was also used to demonstrate that several pore-lining residues in S6 are rapidly modified by MTS reagents faster than when the channel is inactivated or closed (Liu et al., 1997; Panyi and Deutsch, 2006).

The results displayed in Fig. 3 constitute evidence that when the activation gate is closed, no modification of cysteine residues

Table 1. **Gating parameters of T449A/A471C, T449A/L472C, and T449A/P473C//T449 constructs**

	Voltage-dependence of steady-state activation			Voltage-dependence of steady-state inactivation			Inactivation kinetics		RFI	
	$V_{1/2}$ (mV)	s (mV)	*n*	$V_{1/2}$ (mV)	s (mV)	*n*	τ_i (ms)	*n*	τ_{rec} (s)	*n*
T449A/A471C	0.3 ± 2.9	22.3 ± 3.2	6	−52.8 ± 2.2	−7.3 ± 1.2	5	16.3 ± 1.9	23	9.4 ± 0.8	5
T449A/L472C	−26.0 ± 2.0	12.1 ± 1.5	6	−72.5 ± 3.5	−12.6 ± 3.6	5	26.6 ± 2.3	24	4.4 ± 0.7	5
T449A/P473C//T449	−19.0 ± 7.2	17.5 ± 1.9	6	−58.2 ± 4.4	−6.3 ± 2.1	4	$\tau_{i,f}$ = 69.1 ± 6.6 $\tau_{i,s}$ = 595.0 ± 51.0	25	1.8 ± 0.2	5
T449A (Szanto et al., 2021)	−19.8 ± 1.5	14.7 ± 0.8	7	−67.8 ± 3.6	−6.4 ± 0.8	7	103.0 ± 8.0	9	3.7 ± 0.3	8
Shaker-IR (Martinez-Morales et al., 2014)	−28.3 ± 2.8	4.9 ± 0.4		n.a.			n.a.			

$V_{1/2}$ and s values were obtained by the Boltzmann function to the data. The inactivation time constant (τ_i) obtained from single-exponential fits or the time constants for the fast ($\tau_{i,f}$) and slow ($\tau_{i,s}$) components of the decay, obtained from fitting the sum of two exponential terms to the data points, are indicated in the "Inactivation kinetics" column. τ_{rec} is the time constant for recovery from inactivation (RFI), *n* indicates the number of independent experiments. See Materials and methods for the equations used for fitting. Data for the inactivation removed T449A and *Shaker* are from the references indicated in the parentheses; n.a., not applicable.

(471–473) occurs as the hydrophilic MTS molecules are unable to penetrate the membrane. Therefore, the closed activation gate prevents modification of cysteine side chains. In contrast, when the activation gate is open (O state, Fig. 1 C), S6 residues, namely I470C and V474C, are modified by MTS reagents (Liu et al., 1997; Panyi and Deutsch, 2006; Panyi and Deutsch, 2007). Residues 471–473C, however, are inaccessible to cysteine-modifying reagents in the open state of the channels. These findings suggest that only S6 residues facing the water-filled cavity in the open state are available for MTS modification.

In contrast, the accessibility of selected cysteine residues in the OI state of the channels, where the A-gate is still open but the slow inactivation gate is closed (Fig. 1 C), is clearly demonstrated by the progressive decrease of the peak currents when MTSEA was repeatedly applied to the T449A/A471C and T449A/P473C//T449 channels (Figs. 5 and 6). When heteromeric channels were exposed to MTSEA, some of the channels were still in the O state (Fig. 6 C). As P473C in the open state cannot be modified by MTSEA, we argue that the fraction of channels in the open state does not compromise our conclusion that the loss of the current is a consequence of channel modification in the OI state. However, cell-to-cell variability of the inactivation kinetics and the fraction of channels in the MTSEA-modifiable OI state may contribute to the relatively large errors and the complexity of the curve in Fig. 6 D.

The slower modification rate for T449A/A471C and T449A/P473C//T449 compared to T449A/I470C and T449A/V474C may reflect the limited access of 471C and 473C side chains for MTSEA as they face away from the central cavity, but slow inactivation exposes them sufficiently for MTS modification. Similar experiments using 0.2 mM MTSET produced only a negligible current reduction in the inactivated state of the channels. This may be due to the larger size of MTSET (5.8 Å) compared with MTSEA (3.6 Å) rather than the charge or charge delocalization. Moreover, the A471C residues on each subunit are relatively far away from each other as intracellular Cd^{2+} is unable to form crossbridges and block ion conduction (data not shown), a clear contrast to cysteines at positions V474 and I470 where intersubunit Cd^{2+} crossbridges form in both the open and OI states. Consistent with these data, residue L472C, which faces away from the water-filled cavity (see helical wheel, Fig. 1 B), is completely inaccessible to MTS reagents regardless of the state of the gates. The current is not modified by either MTSEA or MTSET in either the O or OI gating states.

A rigid-body rotation of S6 may predict a simultaneous reduction in the accessibility of V474C and I470C and an increase in the accessibility of A471C, whereby A471C is repositioned with respect to the aqueous cavity during a counter-clockwise turn of S6 (see Fig. 1 B). Consequently, the rotation of S6 upon inactivation displaces L472C toward A471C's position in the open state. Thus, L472C is still inaccessible to MTS reagents in the OI state. This rotation scenario would put P473C into an even less accessible position. A plausible explanation for the accessibility of P473C in our study (Fig. 6, C and D) may be that the symmetry of the channel is broken in the P473C heterotetramer (as suggested by the biphasic inactivation kinetics in Fig. 6, C–E). This asymmetry may result in an unexpected exposure of P473C to MTSEA. To our knowledge, our experiments are the first to address the rearrangements of S6 in the inactivated state by systematically substituting amino acids for cysteines along S6 and determining their accessibility to MTS reagents in O vs. OI gating states of the channel. These novel data, combined with previous experiments on the state-dependent accessibility of V474C and I470C, are consistent with the rotation of the S6 helix along its longitudinal axis concomitant with channel entry into the slow inactivated state. Whether this S6 motion is necessary and sufficient to mediate the crosstalk between activation and inactivation gates remains to be elucidated; however, our results provide a mechanistic background for such coupling. Thermodynamic mutant cycle analyses demonstrated that gating-sensitive residues that are as much as 15 Å apart in S6 are coupled to each other (Yifrach and MacKinnon, 2002; Sadovsky and Yifrach, 2007). These residues cluster mainly in the bundle-crossing region of the activation gate and the upstream region where S6 contacts the pore helix. While the underlying interactions responsible for similar coupling during slow inactivation gating in *Shaker* are not known, one possibility is S6 rearrangement, including a rigid-body rotation of S6, which may be dynamically short-lived in the gating transition and therefore not structurally detectable (Tan et al., 2022). Recent cryo-EM structures of *Shaker* corresponding to the O state (*Shaker*-IR) and OI state (W434F mutant of *Shaker*-IR, which renders the channel permanently slow inactivated; Perozo et al., 1993; Yang et al., 1997) show that the S6 helices in these two structures are overlapping. The rotation of the S6 helix along its longitudinal axis, as proposed by us, can be reconciled with the cryo-EM data if we assume that the S6 rotates transiently during the transition between the O and OI states.

There is precedence in the literature for rigid-body rotation of α-helices in several transmembrane proteins, which indicates that this molecular motion is energetically plausible. For example, F α-helices of bacteriorhodopsin undergo helical rigid-body movements during the photocycle (Xiao et al., 2000). Moreover, the rotation of transmembrane helices relative to each other is a concept that appears to supersede the more traditional idea of ligand-induced dimerization of growth factor receptors (Fleishman et al., 2002; Zakany et al., 2020; Kovacs et al., 2022). EPR spectroscopy and a computational strategy also predicted rigid-body movements, including rotation in three dimensions, for the KcsA channel during activation gating (Sompornpisut et al., 2001).

However, movements of side chains independent of the rigid-body motion of α-helical structures were observed when comparing the open and closed structural models of KcsA (Cuello et al., 2010a, 2010b). An alternative explanation of our data, where S6 does not rotate but rather the microenvironment around the helix is altered with consequent changes in S6 cysteine accessibilities, is thus possible. Such a scenario, e.g., global changes in the water-filled cavity upon inactivation, might account for a change in TEA^+ affinity of the inactivated state (Panyi and Deutsch, 2007) and the blocking of $K_V1.3$ by small-molecule inhibitors that bind specifically to the slow-inactivated state (Hanner et al., 2001). Alterations in the microenvironment of S6 residues due to their proximity to the S6 PVPV bend

(del Camino et al., 2000; Webster et al., 2004) may also explain different accessibilities. Moreover, it is also known that there are many channels that manifest 3_{10}-helices and π-bulges during gating transitions, including K_V channels (Villalba-Galea et al., 2008; Infield et al., 2018), calcium-activated Cl^- channels (Paulino et al., 2017), and cyclic-nucleotide-gated channels (Clayton et al., 2008). Another intriguing possibility is that S6 may not be a canonical rigid α-helix in the OI state (but might be rigid both in O and C or CI states), which allows more flexible backbone or side-chain movements during slow inactivation. Moreover, the reactivity of certain residues to MTSEA depends on cysteine ionization, the dielectric of the microenvironment, and proximal charged residues (Linsdell, 2015). All of these determinants can be affected by side-chain rotamerizations and/or altered intersubunit interactions that are induced in different gating states.

Regardless of the coupling mechanism between the two gates, the crosstalk between them will surely affect cell excitability because inactivation governs the amount of available K^+ channels in cells contributing critically to the resting membrane potential and the shape and frequency of the action potential, all of which influence other membrane potential–dependent processes (e.g., neurotransmitter release; Dodson and Forsythe, 2004) and thus, are associated with several neurological and psychiatric disorders (Adelman et al., 1995; Hübner and Jentsch, 2002; Yellen, 2002; Kurata and Fedida, 2006). On the other hand, state-dependent structural changes bear relevance on drug design, as numerous small molecule channel blockers are known to bind to the central cavity of voltage-gated potassium channels, preferentially in the slow-inactivated state. Due to these interactions, understanding the gating transitions of K_V ion channels may also aid in the design of more efficient drug molecules that bind to ion channels in a state-dependent manner. This can be important, e.g., in the development of antiarrhythmic drugs with higher specificity and more favorable state-dependent properties.

In summary, our results support the idea that the rotation of S6 may mediate the communication between the activation gate and the inactivation gate controlling slow inactivation in K_V channels and provide fine details on the contribution of residues lining the cavity to the slow-inactivation gating of *Shaker*.

Data availability

The data are available from the corresponding author upon reasonable request by e-mail communication.

Acknowledgments

Christopher J. Lingle served as editor.

The authors thank Cecilia Nagy and Adrienn Bagosi for their expert technical assistance.

This work was supported by the Hungarian Academy of Sciences projects KTIA_NAP_13-2-2015-0009 and KTIA_NAP_13-2-2017-0013 (to Z. Varga); National Research Development and Innovation Office, Hungary, grants OTKA K132906 (to Z. Varga) and OTKA K143071 (to G. Panyi); Ministry of Human Capacities, Hungary, grant EFOP-3.6.2-16-2017-00006 (to G. Panyi); and Ministry of Finance, Hungary, grant GINOP-2.3.2-15-2016-00044 (to G. Panyi); and National Institutes of Health R01 GM052302 (to C. Deutsch).

Author contributions: T.G. Szanto: Conceptualization, Investigation, Formal analysis, and Writing—Original Draft. F. Papp: Investigation and Formal analysis. F. Zakany: Investigation and Formal analysis. Z. Varga: Conceptualization, Writing—Review & Editing. C. Deutsch: Conceptualization, Writing—Review & Editing, Methodology. G. Panyi: Conceptualization, Writing—Original Draft, Writing—Review & Editing, Funding acquisition, and Methodology.

The authors declare no competing interests exist.

Submitted: 29 January 2023
Revised: 14 April 2023
Accepted: 4 May 2023

References

Adelman, J.P., C.T. Bond, M. Pessia, and J. Maylie. 1995. Episodic ataxia results from voltage-dependent potassium channels with altered functions. *Neuron.* 15:1449–1454. https://doi.org/10.1016/0896-6273(95)90022-5

Baker, O.S., H.P. Larsson, L.M. Mannuzzu, and E.Y. Isacoff. 1998. Three transmembrane conformations and sequence-dependent displacement of the S4 domain in shaker K^+ channel gating. *Neuron.* 20:1283–1294. https://doi.org/10.1016/S0896-6273(00)80507-3

Bernèche, S., and B. Roux. 2001. Energetics of ion conduction through the K^+ channel. *Nature.* 414:73–77. https://doi.org/10.1038/35102067

Bernèche, S., and B. Roux. 2003. A microscopic view of ion conduction through the K^+ channel. *Proc. Natl. Acad. Sci. USA.* 100:8644–8648. https://doi.org/10.1073/pnas.1431750100

Bezanilla, F. 2000. The voltage sensor in voltage-dependent ion channels. *Physiol. Rev.* 80:555–592. https://doi.org/10.1152/physrev.2000.80.2.555

Bezanilla, F., and C.M. Armstrong. 1977. Inactivation of the sodium channel. I. Sodium current experiments. *J. Gen. Physiol.* 70:549–566. https://doi.org/10.1085/jgp.70.5.549

Börjesson, S.I., and F. Elinder. 2011. An electrostatic potassium channel opener targeting the final voltage sensor transition. *J. Gen. Physiol.* 137:563–577. https://doi.org/10.1085/jgp.201110599

Choe, S., and M. Grabe. 2009. Conformational dynamics of the inner pore helix of voltage-gated potassium channels. *J. Chem. Phys.* 130:215103. https://doi.org/10.1063/1.3138906

Clayton, G.M., S. Altieri, L. Heginbotham, V.M. Unger, and J.H. Morais-Cabral. 2008. Structure of the transmembrane regions of a bacterial cyclic nucleotide-regulated channel. *Proc. Natl. Acad. Sci. USA.* 105:1511–1515. https://doi.org/10.1073/pnas.0711533105

Cordero-Morales, J.F., L.G. Cuello, and E. Perozo. 2006a. Voltage-dependent gating at the KcsA selectivity filter. *Nat. Struct. Mol. Biol.* 13:319–1322. https://doi.org/10.1038/nsmb1070

Cordero-Morales, J.F., L.G. Cuello, Y. Zhao, V. Jogini, D.M. Cortes, B. Roux, and E. Perozo. 2006b. Molecular determinants of gating at the potassium-channel selectivity filter. *Nat. Struct. Mol. Biol.* 13:311–1318. https://doi.org/10.1038/nsmb1069

Cordero-Morales, J.F., V. Jogini, S. Chakrapani, and E. Perozo. 2011. A multipoint hydrogen-bond network underlying KcsA C-type inactivation. *Biophys. J.* 100:2387–2393. https://doi.org/10.1016/j.bpj.2011.01.073

Cuello, L.G., D.M. Cortes, and E. Perozo. 2017. The gating cycle of a K^+ channel at atomic resolution. *Elife.* 6:e28032. https://doi.org/10.7554/eLife.28032

Cuello, L.G., V. Jogini, D.M. Cortes, A.C. Pan, D.G. Gagnon, O. Dalmas, J.F. Cordero-Morales, S. Chakrapani, B. Roux, and E. Perozo. 2010a. Structural basis for the coupling between activation and inactivation gates in K^+ channels. *Nature.* 466:272–1275. https://doi.org/10.1038/nature09136

Cuello, L.G., V. Jogini, D.M. Cortes, and E. Perozo. 2010b. Structural mechanism of C-type inactivation in K^+ channels. *Nature.* 466:203–1208. https://doi.org/10.1038/nature09153

del Camino, D., M. Holmgren, Y. Liu, and G. Yellen. 2000. Blocker protection in the pore of a voltage-gated K^+ channel and its structural implications. *Nature*. 403:321–325. https://doi.org/10.1038/35002099

del Camino, D., and G. Yellen. 2001. Tight steric closure at the intracellular activation gate of a voltage-gated K^+ channel. *Neuron*. 32:649–656. https://doi.org/10.1016/S0896-6273(01)00487-1

Ding, S., and R. Horn. 2002. Tail end of the S6 segment: Role in permeation in shaker potassium channels. *J. Gen. Physiol.* 120:87–97. https://doi.org/10.1085/jgp.20028611

Dodson, P.D., and I.D. Forsythe. 2004. Presynaptic K^+ channels: Electrifying regulators of synaptic terminal excitability. *Trends Neurosci.* 27:210–217. https://doi.org/10.1016/j.tins.2004.02.012

Doyle, D.A., J. Morais Cabral, R.A. Pfuetzner, A. Kuo, J.M. Gulbis, S.L. Cohen, B.T. Chait, and R. MacKinnon. 1998. The structure of the potassium channel: Molecular basis of K^+ conduction and selectivity. *Science*. 280:69–77. https://doi.org/10.1126/science.280.5360.69

Fleishman, S.J., J. Schlessinger, and N. Ben-Tal. 2002. A putative molecular-activation switch in the transmembrane domain of erbB2. *Proc. Natl. Acad. Sci. USA*. 99:15937–15940. https://doi.org/10.1073/pnas.252640799

Hackos, D.H., T.H. Chang, and K.J. Swartz. 2002. Scanning the intracellular S6 activation gate in the shaker K^+ channel. *J. Gen. Physiol.* 119:521–532. https://doi.org/10.1085/jgp.20028569

Hamill, O.P., A. Marty, E. Neher, B. Sakmann, and F.J. Sigworth. 1981. Improved patch-clamp techniques for high-resolution current recording from cells and cell-free membrane patches. *Pflugers Arch.* 391:85–100. https://doi.org/10.1007/BF00656997

Hanner, M., B. Green, Y.D. Gao, W.A. Schmalhofer, M. Matyskiela, D.J. Durand, J.P. Felix, A.R. Linde, C. Bordallo, G.J. Kaczorowski, et al. 2001. Binding of correolide to the $K_v1.3$ potassium channel: Characterization of the binding domain by site-directed mutagenesis. *Biochemistry*. 40:11687–11697. https://doi.org/10.1021/bi0111698

Hoshi, T., and C.M. Armstrong. 2013. C-Type inactivation of voltage-gated K^+ channels: Pore constriction or dilation? *J. Gen. Physiol.* 141:151–160. https://doi.org/10.1085/jgp.201210888

Hoshi, T., W.N. Zagotta, and R.W. Aldrich. 1990. Biophysical and molecular mechanisms of Shaker potassium channel inactivation. *Science*. 250:533–538. https://doi.org/10.1126/science.2122519

Hoshi, T., W.N. Zagotta, and R.W. Aldrich. 1991. Two types of inactivation in Shaker K^+ channels: Effects of alterations in the carboxy-terminal region. *Neuron*. 7:547–556. https://doi.org/10.1016/0896-6273(91)90367-9

Hübner, C.A., and T.J. Jentsch. 2002. Ion channel diseases. *Hum. Mol. Genet.* 11:2435–2445. https://doi.org/10.1093/hmg/11.20.2435

Infield, D.T., K. Matulef, J.D. Galpin, K. Lam, E. Tajkhorshid, C.A. Ahern, and F.I. Valiyaveetil. 2018. Main-chain mutagenesis reveals intrahelical coupling in an ion channel voltage-sensor. *Nat. Commun.* 9:5055. https://doi.org/10.1038/s41467-018-07477-3

Karbat, I., H. Altman-Gueta, S. Fine, T. Szanto, S. Hamer-Rogotner, O. Dym, F. Frolow, D. Gordon, G. Panyi, M. Gurevitz, and E. Reuveny. 2019. Pore-modulating toxins exploit inherent slow inactivation to block K^+ channels. *Proc. Natl. Acad. Sci. USA*. 116:18700–18709. https://doi.org/10.1073/pnas.1908903116

Kovacs, T., F. Zakany, and P. Nagy. 2022. It takes more than two to tango: Complex, hierarchal, and membrane-modulated interactions in the regulation of receptor tyrosine kinases. *Cancers*. 14:944. https://doi.org/10.3390/cancers14040944

Kozak, M. 1991. Structural features in eukaryotic mRNAs that modulate the initiation of translation. *J. Biol. Chem.* 266:19867–19870. https://doi.org/10.1016/S0021-9258(18)54860-2

Kurata, H.T., and D. Fedida. 2006. A structural interpretation of voltage-gated potassium channel inactivation. *Prog. Biophys. Mol. Biol.* 92:185–208. https://doi.org/10.1016/j.pbiomolbio.2005.10.001

Labro, A.J., D.M. Cortes, C. Tilegenova, and L.G. Cuello. 2018. Inverted allosteric coupling between activation and inactivation gates in K^+ channels. *Proc. Natl. Acad. Sci. USA*. 115:5426–5431. https://doi.org/10.1073/pnas.1800559115

Larsson, H.P., O.S. Baker, D.S. Dhillon, and E.Y. Isacoff. 1996. Transmembrane movement of the shaker K^+ channel S4. *Neuron*. 16:387–397. https://doi.org/10.1016/S0896-6273(00)80056-2

Li, J., J. Ostmeyer, L.G. Cuello, E. Perozo, and B. Roux. 2018. Rapid constriction of the selectivity filter underlies C-type inactivation in the KcsA potassium channel. *J. Gen. Physiol.* 150:1408–1420. https://doi.org/10.1085/jgp.201812082

Linsdell, P. 2015. Metal bridges to probe membrane ion channel structure and function. *Biomol. Concepts*. 6:191–203. https://doi.org/10.1515/bmc-2015-0013

Liu, X., C. Alexander, J. Serrano, E. Borg, and D.C. Dawson. 2006. Variable reactivity of an engineered cysteine at position 338 in cystic fibrosis transmembrane conductance regulator reflects different chemical states of the thiol. *J. Biol. Chem.* 281:8275–8285. https://doi.org/10.1074/jbc.M512458200

Liu, Y., M. Holmgren, M.E. Jurman, and G. Yellen. 1997. Gated access to the pore of a voltage-dependent K^+ channel. *Neuron*. 19:175–184. https://doi.org/10.1016/S0896-6273(00)80357-8

Liu, Y., M.E. Jurman, and G. Yellen. 1996. Dynamic rearrangement of the outer mouth of a K^+ channel during gating. *Neuron*. 16:859–867. https://doi.org/10.1016/S0896-6273(00)80106-3

Loboda, A., A. Melishchuk, and C. Armstrong. 2001. Dilated and defunct K channels in the absence of K^+. *Biophys. J.* 80:2704–2714. https://doi.org/10.1016/S0006-3495(01)76239-X

López-Barneo, J., T. Hoshi, S.H. Heinemann, and R.W. Aldrich. 1993. Effects of external cations and mutations in the pore region on C-type inactivation of Shaker potassium channels. *Receptors Channels*. 1:61–71.

Lu, Z., A.M. Klem, and Y. Ramu. 2002. Coupling between voltage sensors and activation gate in voltage-gated K^+ channels. *J. Gen. Physiol.* 120:663–676. https://doi.org/10.1085/jgp.20028696

Martinez-Morales, E., D.J. Snyders, and A.J. Labro. 2014. Mutations in the S6 gate isolate a late step in the activation pathway and reduce 4-AP sensitivity in shaker K_v channel. *Biophys. J.* 106:134–144. https://doi.org/10.1016/j.bpj.2013.11.025

Morais-Cabral, J.H., Y. Zhou, and R. MacKinnon. 2001. Energetic optimization of ion conduction rate by the K^+ selectivity filter. *Nature*. 414:37–42. https://doi.org/10.1038/35102000

Ong, S.T., A. Tyagi, K.G. Chandy, and S. Bhushan. 2022. Mechanisms underlying C-type inactivation in Kv channels: Lessons from structures of human Kv1.3 and fly shaker-IR channels. *Front. Pharmacol.* 13:924289. https://doi.org/10.3389/fphar.2022.924289

Ostmeyer, J., S. Chakrapani, A.C. Pan, E. Perozo, and B. Roux. 2013. Recovery from slow inactivation in K^+ channels is controlled by water molecules. *Nature*. 501:121–124. https://doi.org/10.1038/nature12395

Panyi, G., and C. Deutsch. 2006. Cross talk between activation and slow inactivation gates of Shaker potassium channels. *J. Gen. Physiol.* 128:547–559. https://doi.org/10.1085/jgp.200609644

Panyi, G., and C. Deutsch. 2007. Probing the cavity of the slow inactivated conformation of shaker potassium channels. *J. Gen. Physiol.* 129:403–418. https://doi.org/10.1085/jgp.200709758

Panyi, G., Z. Varga, and R. Gáspár. 2004. Ion channels and lymphocyte activation. *Immunol. Lett.* 92:55–66. https://doi.org/10.1016/j.imlet.2003.11.020

Paulino, C., V. Kalienkova, A.K.M. Lam, Y. Neldner, and R. Dutzler. 2017. Activation mechanism of the calcium-activated chloride channel TMEM16A revealed by cryo-EM. *Nature*. 552:421–425. https://doi.org/10.1038/nature24652

Perozo, E., D.M. Cortes, and L.G. Cuello. 1999. Structural rearrangements underlying K^+-channel activation gating. *Science*. 285:73–78. https://doi.org/10.1126/science.285.5424.73

Perozo, E., R. MacKinnon, F. Bezanilla, and E. Stefani. 1993. Gating currents from a nonconducting mutant reveal open-closed conformations in Shaker K^+ channels. *Neuron*. 11:353–358. https://doi.org/10.1016/0896-6273(93)90190-3

Pless, S.A., J.D. Galpin, A.P. Niciforovic, H.T. Kurata, and C.A. Ahern. 2013. Hydrogen bonds as molecular timers for slow inactivation in voltage-gated potassium channels. *Elife*. 2:e01289. https://doi.org/10.7554/eLife.01289

Reddi, R., K. Matulef, E.A. Riederer, M.R. Whorton, and F.I. Valiyaveetil. 2022. Structural basis for C-type inactivation in a Shaker family voltage-gated K^+ channel. *Sci. Adv.* 8:eabm8804. https://doi.org/10.1126/sciadv.abm8804

Renart, M.L., A.M. Giudici, J.A. Poveda, A. Fedorov, M.N. Berberan-Santos, M. Prieto, C. Díaz-García, J.M. González-Ros, and A. Coutinho. 2019. Conformational plasticity in the KcsA potassium channel pore helix revealed by homo-FRET studies. *Sci. Rep.* 9:6215. https://doi.org/10.1038/s41598-019-42405-5

Sadovsky, E., and O. Yifrach. 2007. Principles underlying energetic coupling along an allosteric communication trajectory of a voltage-activated K^+ channel. *Proc. Natl. Acad. Sci. USA*. 104:19813–19818. https://doi.org/10.1073/pnas.0708120104

Schmid, S.I., and S. Grissmer. 2011. Effect of verapamil on the action of methanethiosulfonate reagents on human voltage-gated $K_v1.3$ channels: Implications for the C-type inactivated state. *Br. J. Pharmacol.* 163:662–674. https://doi.org/10.1111/j.1476-5381.2011.01258.x

Sheets, M.F., and D.A. Hanck. 2007. Outward stabilization of the S4 segments in domains III and IV enhances lidocaine block of sodium channels. *J. Physiol.* 582:317–334. https://doi.org/10.1113/jphysiol.2007.134262

Sheng, S., J. Li, K.A. McNulty, T. Kieber-Emmons, and T.R. Kleyman. 2001. Epithelial sodium channel pore region. structure and role in gating. *J. Biol. Chem.* 276:1326–1334. https://doi.org/10.1074/jbc.M008117200

Soler-Llavina, G.J., T.H. Chang, and K.J. Swartz. 2006. Functional interactions at the interface between voltage-sensing and pore domains in the Shaker K_v channel. *Neuron.* 52:623–634. https://doi.org/10.1016/j.neuron.2006.10.005

Sompornpisut, P., Y.S. Liu, and E. Perozo. 2001. Calculation of rigid-body conformational changes using restraint-driven Cartesian transformations. *Biophys. J.* 81:2530–2546. https://doi.org/10.1016/S0006-3495(01)75898-5

Szanto, T.G., S. Gaal, I. Karbat, Z. Varga, E. Reuveny, and G. Panyi. 2021. Shaker-IR K^+ channel gating in heavy water: Role of structural water molecules in inactivation. *J. Gen. Physiol.* 153:e202012742. https://doi.org/10.1085/jgp.202012742

Szanto, T.G., F. Zakany, F. Papp, Z. Varga, C.J. Deutsch, and G. Panyi. 2020. The activation gate controls steady-state inactivation and recovery from inactivation in Shaker. *J. Gen. Physiol.* 152:e202012591. https://doi.org/10.1085/jgp.202012591

Tan, X.F., C. Bae, R. Stix, A.I. Fernández-Mariño, K. Huffer, T.H. Chang, J. Jiang, J.D. Faraldo-Gómez, and K.J. Swartz. 2022. Structure of the Shaker Kv channel and mechanism of slow C-type inactivation. *Sci. Adv.* 8:eabm7814. https://doi.org/10.1126/sciadv.abm7814

Varga, Z., P. Hajdu, G. Panyi, R. Gáspár, and Z. Krasznai. 2007. Involvement of membrane channels in autoimmune disorders. *Curr. Pharm. Des.* 13:2456–2468. https://doi.org/10.2174/138161207781368576

Villalba-Galea, C.A., W. Sandtner, D.M. Starace, and F. Bezanilla. 2008. S4-based voltage sensors have three major conformations. *Proc. Natl. Acad. Sci. USA.* 105:17600–17607. https://doi.org/10.1073/pnas.0807387105

Webster, S.M., D. Del Camino, J.P. Dekker, and G. Yellen. 2004. Intracellular gate opening in Shaker K^+ channels defined by high-affinity metal bridges. *Nature.* 428:864–868. https://doi.org/10.1038/nature02468

Xiao, W., L.S. Brown, R. Needleman, J.K. Lanyi, and Y.K. Shin. 2000. Light-induced rotation of a transmembrane α-helix in bacteriorhodopsin. *J. Mol. Biol.* 304:715–721. https://doi.org/10.1006/jmbi.2000.4255

Yang, Y., Y. Yan, and F.J. Sigworth. 1997. How does the W434F mutation block current in Shaker potassium channels? *J. Gen. Physiol.* 109:779–789. https://doi.org/10.1085/jgp.109.6.779

Yellen, G. 2002. The voltage-gated potassium channels and their relatives. *Nature.* 419:35–42. https://doi.org/10.1038/nature00978

Yellen, G., D. Sodickson, T.Y. Chen, and M.E. Jurman. 1994. An engineered cysteine in the external mouth of a K^+ channel allows inactivation to be modulated by metal binding. *Biophys. J.* 66:1068–1075. https://doi.org/10.1016/S0006-3495(94)80888-4

Yifrach, O., and R. MacKinnon. 2002. Energetics of pore opening in a voltage-gated K^+ channel. *Cell.* 111:231–239. https://doi.org/10.1016/S0092-8674(02)01013-9

Zagotta, W.N., T. Hoshi, and R.W. Aldrich. 1990. Restoration of inactivation in mutants of Shaker potassium channels by a peptide derived from ShB. *Science.* 250:568–571. https://doi.org/10.1126/science.2122520

Zakany, F., T. Kovacs, G. Panyi, and Z. Varga. 2020. Direct and indirect cholesterol effects on membrane proteins with special focus on potassium channels. *Biochim. Biophys. Acta Mol. Cell Biol. Lipids.* 1865:158706. https://doi.org/10.1016/j.bbalip.2020.158706

Zhou, M., and R. MacKinnon. 2004. A mutant KcsA K^+ channel with altered conduction properties and selectivity filter ion distribution. *J. Mol. Biol.* 338:839–846. https://doi.org/10.1016/j.jmb.2004.03.020

Supplemental material

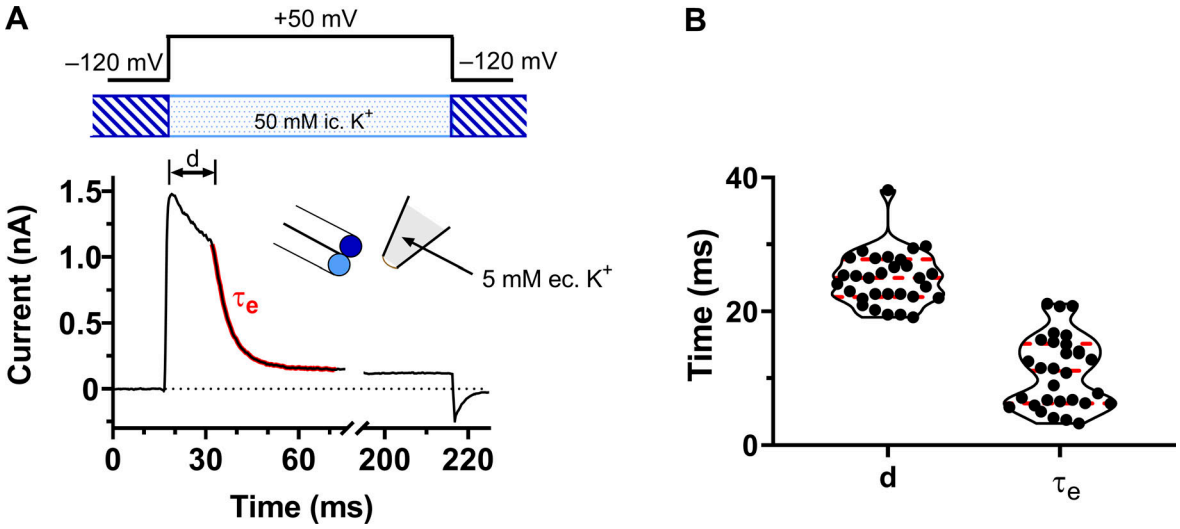

Figure S1. **Characterization of the kinetics of perfusion exchange. (A)** The inside-out patches were held at –120 mV and positioned in the center barrel of the fast perfusion system (see Materials and methods for details). Patches were exposed to 150 mM K^+ (hatched) at the holding potential and then depolarized to +50 mV for 200 ms with a concomitant switch of the barrel to one containing 50 mM K^+ (dotted). The duration of the exposure to 50 mM K^+ was 200 ms. The kinetics of the solution change is depicted in the current trace as a rapid decrease in current. The mechanical and electrical delay is d and the fit of a single exponential to the falling phase of the current (red) gives the time constant of the solution exchange, τ_e. **(B)** Violin plots of d and τ_e show the average values of 24.9 ± 0.7 ms and 10.9 ± 1.0 ms, respectively (n = 30, biological replicates).

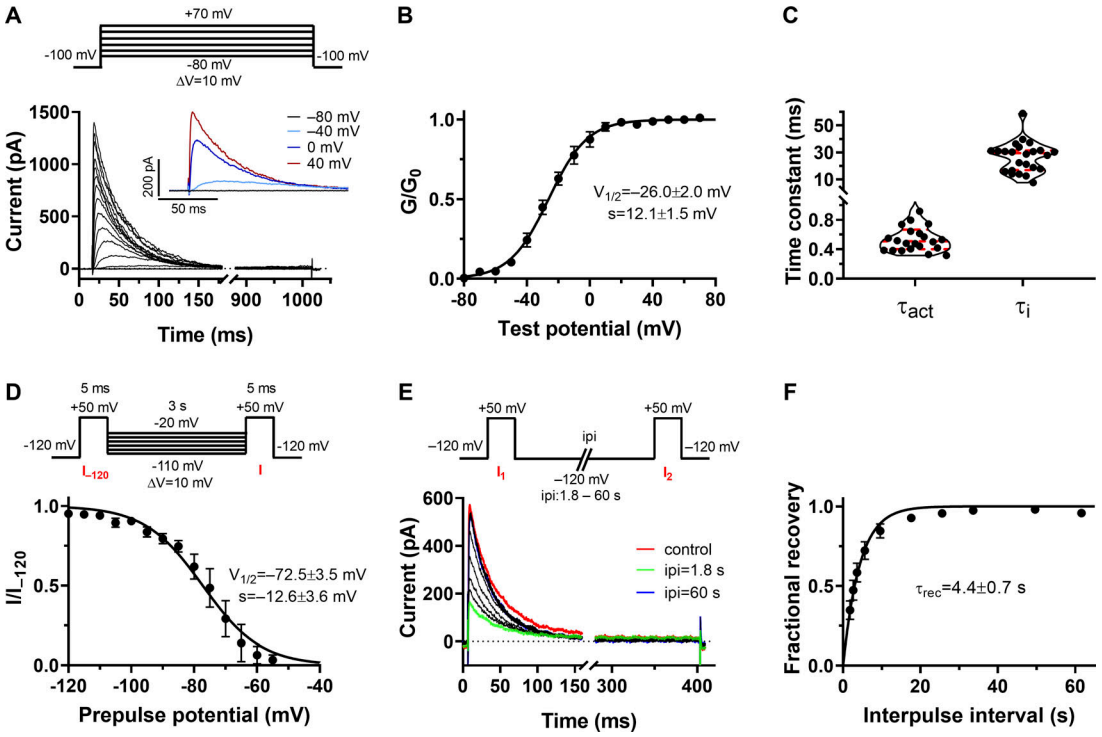

Figure S2. **Biophysical characterization of K⁺ currents evoked in T449A/L472C *Shaker*-IR channel. (A)** The inside-out patch was held at −100 mV and depolarized to test potentials ranging from −80 to +70 mV for 1 s in steps of 10 mV every 60 s. Inset shows K^+ currents evoked by the depolarizing pulses at the indicated test potentials. **(B)** Normalized G–V data were obtained from the peak currents (see Materials and methods for details, averaged, and plotted as a function of test potential). The superimposed solid line shows the best-fit Boltzmann function. The mean values ± SEM of six independent measurements of the midpoint ($V_{1/2}$) and slope factor (s) are shown. **(C)** Activation kinetics were studied using 5-ms-long depolarizing pulse from a holding potential of −120 to +50 mV. Current traces were fitted using Hodgkin–Huxley n^4 model, and the activation time constant (τ_{act}) was determined. Inactivation time constant (τ_i) of the current at +50 mV was determined by fitting a single exponential function to the decaying part of the currents shown in A. Violin plots indicate Q1, median, and Q3 of τ_{act} and τ_i (n = 23), symbols indicate individual data points. **(D)** Voltage dependence of steady-state inactivation was studied using the voltage protocol shown above (see Materials and methods for details). The fraction of nonactivated channels (I/I_{-120}) at each prepulse potential was averaged for n = 5 cells and plotted as a function of prepulse potential. The superimposed solid line is the best-fit Boltzmann function. The mean values ± SEM of the midpoint ($V_{1/2}$) and slope factor (s) are shown. **(E)** Kinetics of recovery from inactivation were determined using pairs of depolarizing pulses from the holding potential of −120 to +50 mV for 400 ms. The ipi at −120 mV varied between 1.8 and 60 s. Control current trace and traces recorded with an ipi of 1.8 and 60 s are highlighted as red, green, and blue, respectively. **(F)** FR was averaged for n = 5 cells and plotted as a function of ipi. The solid line is the best fit with an exponential rise to maximum function yielding the time constant of recovery from inactivation (τ_{rec}). Data are given as mean ± SEM (n = 5), n values are biological replicates in all panels.

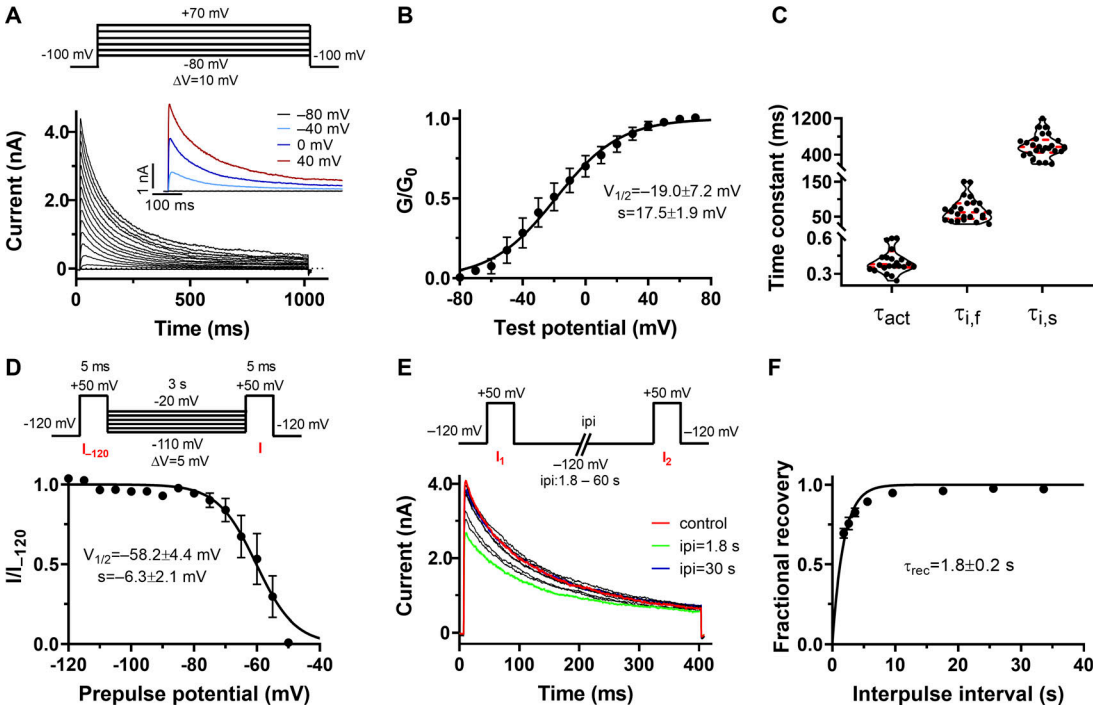

Figure S3. **Biophysical characterization of heteromeric T449A/P473C//T449 *Shaker*-IR channel. (A)** Macroscopic K^+ currents evoked by 1-s-long test potentials ranging from −80 to +70 mV in 10 mV increments every 60 s. Inset shows K^+ currents recorded at the indicated test potentials. **(B)** Averaged normalized G–V data points (see Materials and methods for further description) were plotted as a function of test potential. The superimposed solid line shows the best-fit Boltzmann function. The mean values ± SEM of the midpoint ($V_{1/2}$) and slope factor (s) are shown (n = 6). **(C)** Activation kinetics were studied using 10-ms-long depolarizing pulse from a holding potential of −120 to +50 mV. Current traces were fitted using Hodgkin–Huxley n^4 model, and the activation time constant (τ_{act}) was determined. Inactivation time constants of the current at +50 mV were determined by fitting a double exponential function to the decaying part of the currents shown in A to give time constants of the fast and slow components of slow inactivation, respectively. Violin plots indicate Q1, median, and Q3 of τ_{act}, $\tau_{i,f}$ and $\tau_{i,s}$ (n = 25), and symbols indicate individual data points. **(D)** Voltage dependence of steady-state inactivation was studied using the voltage protocol shown above (see Materials and methods for details). The fraction of nonactivated channels (I/I_{-120}) was plotted as a function of prepulse potential. The superimposed solid line is the best-fit Boltzmann function. The mean values ± SEM of the midpoint ($V_{1/2}$) and slope factor (s) are shown (n = 4). **(E)** Kinetics of recovery from inactivation were determined using pairs of depolarizing pulses from the holding potential of −120 to +50 mV for 400 ms. The ipi at −120 mV varied between 1.8 and 60 s. Control current trace and traces recorded with an ipi of 1.8 and 30 s are highlighted as red, green, and blue, respectively. **(F)** FR was averaged for n = 5 cells and plotted as a function of ipi. The solid line is the best fit with an exponential rise to maximum function yielding the time constant of recovery from inactivation (τ_{rec}). Data are given as mean ± SEM, n values are biological replicates in all panels.

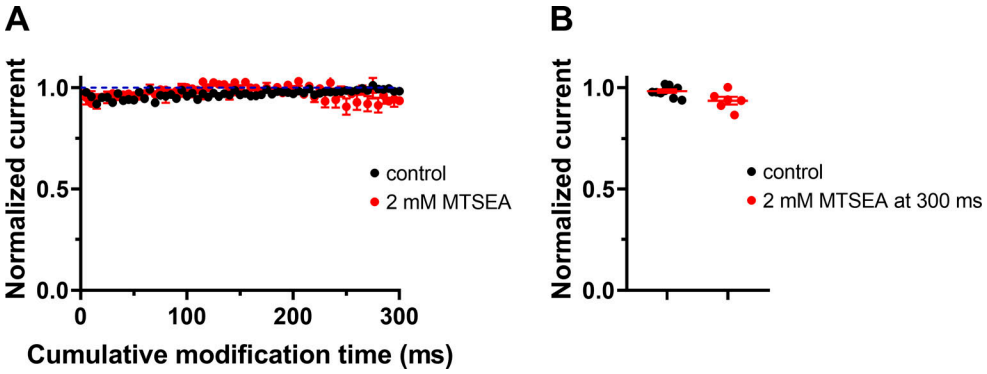

Figure S4. **Application of 2 mM MTSEA to T449A/A471C *Shaker*-IR channel in the open state.** K^+ currents were evoked by 5-ms-long depolarizing pulses from the holding potential of −120 to +50 mV repeated every 10 s in the presence of 2 mM MTSEA in the ICS. For the composition of the solutions see Materials and methods. **(A)** Peak currents for each pulse in the presence of MTSEA (2 mM MTSEA, red symbols; I(t)) were normalized to the last peak current prior to MTSEA application (I_0), averaged, and plotted as a function of cumulative modification time (t). Control currents were recorded in the absence of MTSEA in the ICS, peak currents (I(t)) were normalized to the peak current (I_0) at the beginning of the pulse sequence, averaged, and plotted as a function of cumulative modification time (t; black symbols). **(B)** Normalized peak currents determined at the 60th depolarizing pulse (identical to 300 ms cumulative modification time in 2 mM MTSEA). Symbols indicate individual data points obtained as control (black symbols) and in the presence of 2 mM MTSEA (red symbols). Data are given as mean ± SEM ($n \geq 6$), n values are biological replicates in all panels.